Experimental and theoretical Study of the reactions between neutral vanadium oxide clusters and ethane, ethylene, and acetylene

Feng Dong,[1] Scott Heinbuch,[2] Yan Xie,[1] Jorge J. Rocca,[2] and Elliot R. Bernstein[1*]

[1]Department of Chemistry

[2]Department of Electrical and Computer Engineering,

[1,2]NSF ERC for Extreme Ultraviolet Science and Technology

Colorado State University, Fort Collins, CO 80523, USA

Zhe-Chen Wang[3], Ke Deng[4], and Sheng-Gui He[3*]

[3]Beijing National Laboratory for Molecular Science, State Key Laboratory for Structural Chemistry of Unstable and Stable Species, Institute of Chemistry, Chinese Academy of Sciences, Zhongguancun, Haidian, Beijing 100080, China

[4]National Center of Nanoscience and Technology, Beijing 100080, P. R. China

Abstract

Reactions of neutral vanadium oxide clusters with small hydrocarbons, C_2H_6, C_2H_4, and C_2H_2, are investigated by experiments and density function theory (DFT) calculations. Single photon ionization through extreme ultraviolet (EUV, 46.9 nm, 26.5 eV) and vacuum ultraviolet (VUV, 118 nm, 10.5 eV) lasers is used to detect neutral cluster distributions and reaction products. The most stable vanadium oxide clusters V_xO_y (e.g. VO_2, V_2O_5, V_3O_7, and V_4O_{10}) tend to associate with C_2H_4 generating products $V_xO_yC_2H_4$. Oxygen rich clusters V_xO_{y+1} (x = 1, 3, 5…, e.g., VO_3, V_3O_8, and V_5O_{13}) react with C_2H_4 molecules to cause a cleavage of the C=C bond of C_2H_4 to produce $V_xO_yCH_2$ clusters. For the reactions of vanadium oxide clusters (V_mO_n) with C_2H_2 molecules, $V_mO_nC_2H_2$ are assigned as the major products of the association reactions. Additionally, a dehydration reaction for VO_3 + C_2H_2 to produce VO_2C_2 is also identified. C_2H_6 molecules are quite stable toward reaction with neutral vanadium oxide clusters. Density functional theory calculations are employed to investigate association reactions for V_2O_5 + C_2H_x. The observed relative reactivity of C_2 hydrocarbons toward neutral vanadium oxide clusters is well interpreted by using the DFT calculated binding energies. DFT calculations of the pathways for VO_3+C_2H_4 and VO_3+C_2H_2 reaction systems indicate that the reactions VO_3+C_2H_4→ VO_2CH_2 + H_2CO and VO_3+C_2H_2→ VO_2C_2 + H_2O are thermodynamically favorable and overall barrierless at room temperature, in good agreement with the experimental observations.

1. Introduction

Transition metal oxide materials have been widely applied in the petroleum, chemical, and environmental industries as heterogeneous catalysts and catalytic supports.[1-7] Vanadium oxides are important transition metal oxide catalysts, both by themselves and deposited on the surface of other oxide supports.[8,9] Vanadium oxide based catalysts are used in the manufacture of important chemicals; for example, in the oxidation of SO_2 to SO_3 in the production of sulfuric acid,[10] in selective oxidation of hydrocarbons, and partial oxidation of methane to formaldehyde, etc.[11] A detailed understanding of heterogeneous catalysis at an atomic, mechanistic, electronic state level is still not available; however, gas phase studies of transition metal oxide cluster reactions can provide insight into the mechanism of elementary reactions in catalytic processes at an atomic and molecular level.[12,13,14,15] Gas phase clusters are considered to be an ideal model system for local active sites of condensed/surface phases since they have relatively well defined structures, size dependent properties, and they are readily accessible by theory.[3,16,17,18] On the other hand, full understanding of catalytic behavior of gas phase clusters can in principle provide insight into the mechanism of practical catalyst systems and their design and synthesis.

The reactions of transition metal oxides in particular with hydrocarbons are of interest because of their importance in catalytic processes. These reactions involve C-H and C-C bond activation followed by elimination of hydrogen and small alkane groups.[19-21] The cleavage of C-C bonds by heterogeneous catalysts is a key step in the process of larger hydrocarbons cracking into smaller molecules for the generation of petroleum based products. Vanadium oxides are one of the most important catalysts used in these industrial catalytic processes. To explore the detailed mechanism of these reactions at an atomic and molecular level, the reactivity of vanadium oxide cluster ions with small hydrocarbon compounds has been studied in the gas phase using mass spectrometric techniques[22-32] in conjunction with theoretical studies.[33-40] The reaction of mass selected $V_4O_{10}^+$ with CH_4 has been studied by Feyel and co-workers[24] using a quadrupole based mass spectrometer coupled with an electrospray ionization (ESI) source. They identify a C-H bond activation reaction, $V_4O_{10}^+ + CH_4 \rightarrow V_3O_9OH^+ + CH_3$, employing experiments and theoretical calculations. They also studied the gas phase oxidation of propane (C_3H_8)

and 1-butene (C_4H_8) by the $V_3O_7^+$ cluster ion. Oxidative dehydrogenation (ODH) of hydrocarbons by $V_3O_7^+$ is identified as a major reaction channel, while a minor channel involving C-C bond cleavage to produce $V_3O_7(C_2H_4)^+$ is also observed.[41] The reactions of mass selected $V_mO_n^+$ with ethane (C_2H_6) and ethylene (C_2H_4) were investigated by guided ion beam mass spectroscopy coupled with a laser ablation source.[25,28,33] The major reaction channels observed in these experiments are associations and oxygen transfers. Oxygen transfer reaction pathways are identified for $(V_2O_5)^+_{n=1,2,3}$ cations reacting with C_2H_4 and C_2H_6 molecules. Calculations provide evidence that oxygen transfer reaction pathways are the most energetically favorable for $V_2O_5^+$ and $V_4O_{10}^+$ reacting with C_2H_4 via a radical cation mechanism. The reactions of $V_mO_n^-$ anions with C_2H_4 and C_2H_6 were also investigated, but no reaction products were found.[25]

Most efforts to elucidate the properties and behavior of metal oxide clusters deal with ionic systems because cluster ions can be made directly from an ablation source and selected through some sort of mass filter (e.g. time-of-flight, quadrupole, magnetic sector, etc.). Additionally, ionic clusters represent a model of some suggested defect sites in solids. In order to elucidate in detail the molecular mechanism of reactions between vanadium oxide clusters and hydrocarbons, many theoretical studies have been carried out, but most of these studies also focus on cluster ion reactions related to experimental results.[23,24,28, 33-34, 41-43] Nonetheless, cluster ions are clearly much more reactive than their condensed phase analogues and neutral molecules because of their net charge.[34, 44, 45]

Dobler et al.[34] studied the oxidation of methanol to formaldehyde on silica supported vanadium oxide by density functional theory (DFT). They conclude that the mechanism for the radical cation and the neutral molecule reaction is the same, but that the energy profile changes substantially. The enthalpy changes from endothermic for the neutral molecule to exothermic for radical cation, and the energy barrier is lowered by as much as 70 kJ/ mol for the ionic reaction with respect to that of the neutral reaction. Thus, neutral clusters may be the best representation of true catalytic reaction sites on metals or metal oxide surfaces in bulk/condensed phase systems. Neutral clusters are, however, more difficult to study because they cannot be size selected and one must find a valid method to ionize neutral species without fragmentation, especially for metal oxide clusters with high ionization energies (IE). For example, the IEs of vanadium oxide

clusters are around 8-10 eV or even higher for oxygen rich clusters (e.g., VO_3, V_3O_8,…).[46] Typical multi-photon and electron impact ionization techniques almost always cause severe cluster fragmentation, and thus loss of original neutral cluster information.

Recently, a new desk-top, 26.5 eV/photon (46.9 nm), soft x-ray (extreme ultraviolet, EUV) laser has been employed to study gas phase cluster chemistry in our group. Using this radiation, all the species of neutral metal oxide clusters and the products that are generated from the reactions of metal oxide clusters and reactants can be detected. The soft x-ray laser not only ionizes all the neutral clusters in these experiments, but it is a very gentle ionization source that does not seriously fragment metal oxide clusters (e.g. vanadium, niobium, and tantalum oxide clusters) of interest[47] and even weakly bound $(H_2O)_n$, $(CH_3OH)_n$, $(NH_3)_n$, $(SO_2)_n$, and $(CO_2)_n$ van der Waals and hydrogen bonded clusters.[48-51] In studies of neutral V_mO_n, Nb_mO_n, and Ta_mO_n clusters[47], cluster distributions obtained by 26.5 eV soft x-ray ionization are much the same as those distributions obtained with near threshold ionization by a 118 nm laser, with the exception that some oxygen rich clusters can not be ionized by the 118 nm light. So, the 26.5 eV, soft x-ray laser is an ideal light source with which to study neutral metal oxide cluster reactions. With this ionization source we can detect all neutral cluster species and their reaction products.

In the present work, neutral vanadium oxide clusters are reacted with the C_2 hydrocarbons, C_2H_6, C_2H_4, and C_2H_2. Reactants and products in these reactions are investigated by single photon ionization at 26.5 eV (46.9 nm) and 10.5 eV (118nm). The most stable vanadium oxide clusters V_xO_y (e.g. VO_2, V_2O_5, V_3O_7, and V_4O_{10}) undergo association reactions with C_2H_4 to form products $V_xO_yC_2H_4$. Neutral oxygen rich vanadium oxide clusters with an odd number of vanadium atoms V_xO_{y+1} (e.g. VO_3, V_3O_8, and V_5O_{13}) can react with C_2H_4 molecules to cleave the C=C bond of C_2H_4 and to produce $V_xO_yCH_2$ products. For the reactions of V_mO_n (general) clusters with C_2H_2 molecules, the association complexes $V_mO_nC_2H_2$ are assigned as the major reaction products. Additionally, a dehydration reaction channel is identified for the reaction $VO_3 + C_2H_2 \rightarrow VO_2C_2 + H_2O$. C_2H_6 molecules are not very reactive with neutral vanadium oxide clusters. In order to interpret experimental observations, DFT calculations are

performed to study C_2 hydrocarbon association with V_2O_5 and the pathways for the reactions $VO_3 + C_2H_4$ and $VO_3 + C_2H_2$. DFT calculated results for these reactions are in a good agreement with experimental observations.

2. Experimental Procedures

Experiments performed for this study of neutral cluster reactions involve a time of flight mass spectrometer (TOFMS) coupled with single photon ionization of reactants and products by two different lasers: photon energies 26.5 eV and 10.5 eV. Since the experimental apparatus has been described in detail elsewhere,[46-57] only a general outline of the experimental scheme will be presented in this report. Briefly, the neutral vanadium oxide clusters are generated in a conventional laser vaporization/supersonic expansion cluster source by laser ablation of vanadium foil into a carrier gas of 0.5% O_2 and He at 80 psig. A 532 nm wavelength laser (second harmonic of a Nd/YAG laser, 1064 nm) is employed to ablate the vanadium metal at 10-20 mJ/pulse. The reactant gases, pure C_2H_6, C_2H_4, and C_2H_2, or their mixtures with He, are pulsed into the reactor tube located at 20 mm downstream from the exit of the expansion channel. The generated vanadium oxide clusters react with reactant gases in the flow tube reactor.[58] Neutral clusters and reaction products pass through a skimmer with a 4 mm aperture into the ionization region of a time of flight mass spectrometer (Wiley-McLauran design, R.M. Jordan Co.). The neutral species are ionized by either a 118 nm (ninth harmonic of a seeded Nd/YAG 1064 nm laser[54]) or a 46.9 nm EUV laser[59]. Ion signals generated from laser ionization are detected by a microchannel plate (MCP). In the 118 nm experiments, a two chambered system is used to ensure that the TOFMS chamber pressure is low enough (10^{-5} Torr) for the MCP valtages and the TOFMS mean free path for ions. In this case, the reactant gases are diluted in He (5% ~ 20% C_2H_x/He) and are pulsed into the reactor. The instantaneous reactant gas pressure in the reactor cell is about 20 Torr so that good cooling is achieved for the neutral metal oxide clusters generated in the ablation source. 26.5 eV experiments are carried out in a single chamber system. Pure reactant gases are used in these experiments. The instantaneous reactant gas mixture pressure in the reactor cell is about 1 Torr in this set up. Neutral cluster temperatures in 26.5 eV experiments are higher than those in the 118 nm experiments. Since different experimental conditions and ionization

cross sections exist for these different wavelength experiments, some small difference in the observation of reaction products are found for the 10.5 and 26.5 eV experiments.

The EUV laser (26.5 eV/photon energy) emits pulses of about 1 ns duration with an energy/pulse of 10 μJ at a repetition rate of up to 12 Hz. A pair of gold coated torodial and plane mirrors is placed in a Z-fold configuration just before the ionization region of the TOFMS to provide alignment and focusing capabilities for the laser with respect to the molecular beam at the ionization region. Compared to the spherical mirrors used previously,[47-51] the transmissivity of this Z-fold mirror system increases to about 60% from about 10%. EUV laser light is not tightly focused in ionization region to avoid multiphoton ionization and a space charge Coulomb effect due to He^+ ions. A large number of He^+ ions, produced by 26.5 eV ionization of He in the molecular beam, can broaden the mass spectral features. Since a 26.5 eV photon from the EUV laser is able to ionize the He carrier gas employed in the expansion, the MCP ion detector voltage is gated to reduce the MCP gain when He^+ arrives at the mass detector, in order to prevent detector circuit overload and saturation.

The 118 nm laser light is generated by focusing the third harmonic (355 nm, ~30 mJ/pulse) of a Nd:YAG laser in a tripling cell that contains about a 250 Torr argon/xenon (10/1) gas mixture. To separate the generated 118 nm laser beam from the 355 nm fundamental beam, a magnesium fluoride prism (apex angle = 6 deg), which was not employed in our previous studies,[52-55] is inserted in to the laser beams. In this case, one is quite sure that the mass signals are generated by ionization purely through the VUV laser radiation at low power (~1 μJ/pulse, pulse duration ~5 ns).

3. Computational methods

DFT calculations are carried out using the Gaussian 03 program.[60] The B3LYP functional[61-63] and TZVP basis set[64] are used. B3LYP/TZVP level of theory with moderate computational cost was tested to give reasonably good results for bond strengths of vanadium oxides.[33] The enthalpies of formation for C_2 hydrocarbons are also very well calculated at this level of theory. Binding energies between neutral V_2O_5 and C_2 hydrocarbons are calculated at different typical association geometries. This involves geometry optimizations and vibrational frequency calculations for V_2O_5, C_2 hydrocarbons, and their association products. Extended calculations are performed to find possible

(thermodynamically allowed) reaction channels and pathways for two reaction systems, VO_3 + C_2H_4 and VO_3 + C_2H_2. For each reaction channel, the calculation involves geometry optimization of various reaction intermediates and transition states through which the intermediates transfer to one another. Transition state optimizations are performed by using the Berny algorithm[65] or the synchronous transit-guided quasi-Newton (STQN) method[66, 67]. Vibrational frequency calculations are performed to check that reaction intermediates and transition state species have zero and one imaginary frequencies, respectively. Intrinsic reaction coordinate (IRC) calculations[68, 69] are also performed so that a transition state connects two appropriate local minima in the reaction pathways. The relaxed potential energy surface (PES) scan implemented in Gaussian 03 is extensively used to get good initial structures for the stable and transition states determined. In this method, once a stable state is found, several relaxed PESs can be scanned for possible internal reaction coordinates. The maximum and new minimum in a relaxed PES correspond to good guesses for transition and new stable states, respectively. A complete reaction pathway will be eventually determined following this method. Binding energies are calculated for a few species employing the Basic Set Superposition Error (BSSE) correction:[70] these are found to be insignificant at the present level of theory.

4. Experimental Results

4.1. V_mO_n cluster distribution generated at low oxygen concentration

In our previous studies, vanadium oxide clusters (V_mO_n) are classified into three categories. The first category is the most stable neutral clusters for each V_m family labeled as V_xO_y, such as VO_2, V_2O_4/V_2O_5, V_3O_7, V_4V_{10}, V_5O_{12}, V_6O_{15}, etc. They dominate the cluster distribution in the mass spectrum under saturated oxygen concentration conditions (5% O_2/He expansion), and they have stable structures as demonstrated experimentally and theoretically.[47,71,72] The second category is oxygen rich clusters ($V_xO_{y+1,2}$) that have one or more oxygen atoms compared to the most stable clusters, such as VO_3, V_2O_6, V_3O_8, V_5O_{13}, etc. These clusters present a higher tendency to lose O or O_2 and become the most stable clusters.[72] The third category is oxygen deficient clusters ($V_xO_{y-1,2,3}$) that have one or more oxygen atoms fewer than the most

stable clusters, such as V_2O_3, $V_3O_{5,6}$, $V_4O_{8,9}$. These clusters present a higher tendency to react with O or O_2 and become the most stable clusters.[72]

Figure 1 displays a TOF mass spectrum of V_mO_n clusters generated under a low oxygen concentration condition (0.5% O_2/He expansion) using a 26.5 eV soft x-ray laser for ionization. The predominant TOFMS signals are assigned as VO_2, V_2O_4, V_3O_7, V_4O_{10}, V_5O_{12}, etc. for this expansion. Usually V_2O_5 is considered as a most stable cluster for the V_2O_y group. In our previous experiments, the vanadium oxide clusters are generated under saturated O_2 conditions (5% O_2/He expansion); however, the $V_2O_4^+$ signal is much more intense than the $V_2O_5^+$ signal with 26.5 eV laser ionization. This result is contrary to the result obtained by 118 nm ionization, for which the $V_2O_5^+$ TOFMS feature is much more intense than the $V_2O_4^+$ one. This behavior does not occur for Ta_2O_y and Nb_2O_y clusters; in those distributions, M_2O_5 is the predominant signal in the mass spectra using 26.5 eV ionization.[47] This anomalous behavior is probably most readily associated with the specific details of wavelength dependent ionization cross sections for V_2O_4 and V_2O_5 neutral clusters.

A number of oxygen deficient clusters (V_xO_{y-m}, $V_2O_{2,3}$, $V_3O_{5,6}$, $V_4O_{8,9}$, $V_5O_{9,10,11}$, and $V_6O_{13,14}$) are observed in the cluster distribution since the clusters are generated under a low O_2 concentration condition (see Figure 1). Growth of neutral clusters is kinetically controlled by various processes, such as diffusion, temperature, expansion pressure,… In the experiment, oxygen rich clusters (V_xO_{y+1}, such as VO_3, V_2O_6, V_3O_8, V_5O_{13}, V_7O_{18}) are also observed in the mass spectrum. Additionally, one can find some clusters with one or two hydrogen atoms, such as $VO_3H_{1,2}$, $V_2O_6H_{1,2}$ and $V_3O_8H_{1,2}$ etc. They are generated from oxygen rich clusters that react with trapped hydrogen in the metal or water in the system to produce $V_xO_{y+1}H_{1,2}$. Since the most stable oxidation states for vanadium are +4 and +5, VO_3, V_2O_6, and V_3O_8 etc, can readily form OH ligands to generate these preferred valence states. The same observations are also found for tantalum and niobium oxide clusters.[47] If vanadium oxide clusters are generated under oxygen saturation conditions (5%O_2/He expansion gas), the population of the most stable clusters and oxygen rich clusters will increase in the cluster distribution.[47] Apparently, such oxygen rich clusters tend to be quite reactive.

4.2. Reactions of V_mO_n clusters with C_2H_6

To study neutral V_mO_n cluster reactions with hydrocarbons, the reactants, pure or diluted (in He), ethane (C_2H_6), ethylene (C_2H_4), and acetylene (C_2H_2) gases are individually and separately pulsed into the reactor. When the neutral clusters generated from the ablation/expansion source pass through the reactor cell, collisions will occur between neutral V_mO_n clusters and the hydrocarbons. The instantaneous reactant gas pressure in the reactor cell (during the time that V_mO_n is in the cell) is estimated to be ~ 20 Torr in the case that C_2 hydrocarbons are diluted in He carrier gas. The pressure is about 1-2 Torr in the case that pure C_2 hydrocarbons are used. A new distribution of neutral clusters and reaction products is obtained by using 26.5 or 10.5 eV laser ionization. As shown in Figures 2 and 3, all the cluster signals decrease in roughly the same proportion when C_2H_6 gas is added reactor cell. A similar result is also observed when inert gases are added to the reactor cell. Therefore, the decrease of cluster signals is due to scattering by the C_2H_6 gas pulsed into the reactor. A new product $V_2O_5C_2H_6$ with a weak TOF signal is observed in the 118 nm experiment. Oxygen rich clusters, VO_3, V_3O_8, V_5O_{13}, etc. are not detected by 118 nm ionization due to the high ionization energy of these clusters.[47]

4.3. Reactions of V_mO_n clusters with C_2H_4

As shown in Figure 4(a, b), the major products of the reaction $V_mO_n + C_2H_4$ are assigned as VOC_2H_4, $VO_2C_2H_4$, $V_2O_5C_2H_4$, and $V_3O_8C_2H_4$ generated from an association reaction channel,

$$V_mO_n + C_2H_4 \rightarrow V_mO_nC_2H_4 \quad (1)$$

The reaction products VO_2CH_2, $V_3O_7CH_2$, and $V_5O_{12}CH_2$ are also observed in the mass spectrum. They must be produced from reactions that involve the cleavage of the C=C bond of C_2H_4. A close inspection of the mass regions around the clusters VO_3, V_3O_8, and V_5O_{13} (Figure 4 (c,d,e)) shows that VO_3, V_3O_8 and V_5O_{13} signals have disappeared; this indicates that these oxygen rich clusters react with C_2H_4. The possible reaction channels corresponding to the disappearance of VO_3, V_3O_8 and V_5O_{13} signals and the generation of VO_2CH_2, $V_3O_7CH_2$ and $V_5O_{12}CH_2$ product signals will be discussed in the next section. The reaction of $V_mO_n + C_2H_4$ is also studied using the 118 nm laser ionization, as shown

in Figure 5. Most of the association products observed are similar to those found by the 26.5 eV ionization experiment. Also note that VO_2CH_2 and $V_3O_7CH_2$ products are observed by both 118 nm and 26.5 eV ionization.

4.4. Reaction of V_mO_n clusters with C_2H_2

When C_2H_2 gas is added to the reactor, many new product signals, formed in the reaction of $V_mO_n + C_2H_2$, are observed in the mass spectra, as shown in Figure 6(a, b). The major products, $VO_2C_2H_2$, $VO_3C_2H_2$, $V_2O_5C_2H_2$, $V_3O_8C_2H_2$, $V_4O_{10}C_2H_2$, etc., are generated from the association reactions,

$$V_mO_n + C_2H_2 \rightarrow V_mO_nC_2H_2 \quad (2)$$

For some products, such as $V_3O_9C_2H_2$, $V_4O_{11}C_2H_2$, and $V_5O_{14}C_2H_2$, present in the mass spectrum of $V_mO_n + C_2H_2$, the precursor reactants, V_3O_9, V_4O_{11} and V_5O_{14}, are not observed in the distribution of neutral V_mO_n clusters. Note, however, that hydrogen containing, oxygen rich clusters, such as $V_2O_5H_{1,2}$, $V_2O_6H_2$, $V_3O_8H_{1,2}$, etc, are observed. The absence of these neutral clusters implies that C_2H_2 can stabilize some neutral oxygen rich clusters, avoiding fragmentation during the 26.5 eV ionization process. Additionally, two new products, VO_2C_2 and $VO(C_2H)_2$, are found. These species may arise from dehydration reactions between VO_3 and C_2H_2 and VO_2 and $2C_2H_2$. The different reaction products observed in the 118 nm experiment (see Figure 7) are $V_2O_3C_2H_2$, $V_3O_6C_2H_2$, and $V_4O_9C_2H_2$ and some secondary association products such as $VO_2(C_2H_2)_2$, $V_2O_3(C_2H_2)_2$, and $V_2O_5(C_2H_2)_2$, most probably due to the difference in experimental conditions between the 118 nm and the 26.5 eV experiments, as discussed in experimental section. Additionally, some relatively weak association products may be fragmented by 26.5 eV ionization while they might survive in the 118 nm experiment due to near threshold ionization.

5. DFT Results

5.1 Association products $V_2O_5C_2H_2$, $V_2O_5C_2H_4$, and $V_2O_5C_2H_6$

Figure 8 presents the DFT optimized geometries of association products $V_2O_5C_2H_x$ (x = 2, 4, 6) in three types (A, B, C) of typical configurations. In the type A configuration, the two carbon atoms of C_2H_x connect with O and V atoms of V_2O_5 to

form C-O and C-V bonds, respectively. In the type B configuration, the two carbon atoms connect with two oxygen atoms which are bonded to the two different V atoms of V_2O_5. Two C-O bonds are formed in this type of product. In the type C configuration, two O-C bonds are formed, but both O atoms are connected to the same V atom. In the calculations, binding energies listed below each geometry are defined as $E(V_2O_5$, singlet) + $E(C_2H_x)$ - $E(V_2O_5C_2H_x$, singlet / triplet). The V_2O_5 lowest triplet state is 0.71 eV higher in energy than its singlet ground state at this level of theory. The association species in singlet and triplet spin states are considered. The association reaction happens at near room temperature, so the binding energy is defined with V_2O_5 in the singlet state although the products may eventually be in the triplet state by a spin-inversion mechanism.[73] Two tendencies are found for these binding energies: 1. for each geometry type and each spin multiplicity, the binding energy increases as the hydrocarbon becomes more unsaturated; 2. for unsaturated hydrocarbons C_2H_4 and C_2H_2, the binding energy of the singlet state decreases as the geometry type changes from A to B to C, while the binding energy of the triplet state increases. This behavior can be explained through the valance shell structure and oxidation state of vanadium atoms in these three types of configurations. In the type A geometry, two V atoms are in their most stable +5 state (terminal VO is a double bond), so the singlet state can be more stable than the triplet state when all valence electrons are bonded. In the type B geometry, one V atom is in the +5 state and the other is in the +3 state. In the type C geometry, both V atoms are in the +4 state. Therefore, in type B and C configurations the singlet state is less stable than the triplet state.

5.2 Reaction of VO_3 with C_2H_4 and C_2H_2

DFT calculations are performed for VO_3 cluster reactions with C_2H_4 and C_2H_2. The following reactions are calculated:

$$VO_3 + C_2H_4 \rightarrow VO_2CH_2 + CH_2O \qquad \Delta H_{298} = -0.25 \text{ eV} \quad (3a)$$

$$\rightarrow VO_2 + CH_3CHO \qquad \Delta H_{298} = -0.83 \text{ eV} \quad (3b)$$

$$\rightarrow VO_2{+}CH_2{=}CHOH \qquad \Delta H_{298} = -0.35 \text{ eV} \quad (3c)$$

$$VO_3 + C_2H_2 \rightarrow VO_2C_2 + H_2O \qquad \Delta H_{298} = -0.59 \text{ eV} \quad (4a)$$

$$\rightarrow VO_2 + CH_2CO \qquad \Delta H_{298} = -1.6 \text{ eV} \quad (4b)$$

The values of the enthalpies of reactions (as given above) are obtained for the lowest energy structure of the reactants and products in their singlet or doublet spin states. These reactions are all thermodynamically allowed; however, they may not take place at room temperature due to dynamic constraints. For example, barriers for the oxygen/hydrogen transfer and structure transformation, etc. may be quite high.

Figure 9 presents the DFT calculated relative Gibbs free energies at 298 K for various intermediates and transition states for reactions (3a) and (3b). The optimized geometries of reaction intermediates and transition states are displayed in Figures 10 and 11, respectively. Several reaction channels are found for product **P1** (H_2CO and VO_2CH_2) and **P2** (VO_2 and CH_3CHO) generation:

R1 → 10 → 10/4 → 4 → 4/5 → 5 →5/6 → 6 → 6/7 → 7 → P1 Channel (Ia)

R1 → 1 → 1/2 → 2 → 2/3 → 3 →

3/4 → 4 → 4/5 → 5 → 5/6 → 6 → 6/7 → 7 → P1 Channel (Ib)

3/5 → 5 → 5/6 → 6 → 6/7 → 7 → P1 Channel (Ic)

3/8 → 8 → 8/7 → 7 → P1 Channel (Id)

3/8 → 8 → 8/9 → 9 → 9/7 → 7 → P1 Channel (Ie)

3/4 → 4 → 11 → P2 Channel (IIa)

3/11 → 11 → P2 Channel (IIb)

3/5 → 5 → 5/11 → 11 → P2 Channel (IIc)

3/4 → 4 → 4/5 → 5 → 11 → P2 Channel (IId)

R1 →10 → 10/11 → 11 → P2 Channel (IIe)

The approach of C_2H_4 to the neutral VO_3 cluster from the metal side to form intermediate **1** is a barrierless process. A four-membered ring containing C-O and C-V bonds forms in the immediate **2** via a transition state **1/2**. Through transition state **2/3**, the C-V bond breaks to form intermediate **3**. Starting from intermediate **3**, several possible reaction pathways are found to produce the final product **P1** (CH_2O + VO_2CH_2). C_2H_4 can also attack an O atom of VO_3 to form intermediate **10**, and then transfer to **4** via transition state **10/4**. Intermediate **4** can isomerize to **3** via a transition state **3/4**. In Figure 9, channels (Ia), (Ib), and (Ic) are overall barrierless pathways, in which a lowest energy intermediate **5** (-2.2 eV), a five membered ring (Figure 10), is formed. Note that intermediate **5** containing two C-O bonds, is different from intermediate **2** (C-O-V-C four

membered ring). Through transition state **5/6**, the C-C bond of **5** ruptures and yields intermediate **6** ($CH_2VO_3CH_2$), in which two CH_2 radicals connect with two O atoms of VO_3 by C-O bonds. In intermediate **7**, the formation of a V-O-C three membered ring weakens and stretches the V-O bond between the H_2CO moiety and the VO_2CH_2 moiety from 1.31 Å in **6** to 1.90 Å in **7**, and finally results in product **P1**. About 1 eV energy is required for breaking the V-O bond in this step. The large amount (> 2 eV) of heat released from the formation of the most stable intermediate **5** is enough to overcome any barrier in the steps from intermediate **5** to product **P1**. High barriers (about 0.5 eV) are found for reaction channels (Id) and (Ie): these channels can be open under high temperature conditions.

The formation of product **P2** (CH_3CHO + VO_2, reaction (3b)) is also thermodynamically favorable by 0.83 eV; however, obvious overall barriers exist in reaction channels (IIa-e) as shown in Figure 9. All the reaction channels (IIa-e) involve a hydrogen transfer from one carbon to another carbon during the structure changes from intermediates **3**, **4**, **5**, and **10** to **11.** The barrier heights of transition state **3/11**, **4/11**, **5/11**, **10/11** are about 0.18~0.26 eV, higher than the energy of reactant **R1**. Therefore, reaction (3b) can occur as a high temperature reaction, although the overall reaction is exothermic. We also calculate another possible pathway for a hydrogen transfer from carbon (intermediates **3**, **4**, **5** and **10**) to oxygen to form vinyl alcohol (acetaldehyde) as reaction (3c). It is also an exothermic reaction; however, the barriers are higher than the reactant **R1** energy. Based on calculations, we conclude that the C-C bond breaking reaction (reaction 3a) is more favorable than the oxygen transfer reactions (3b) and (3c), and channels (Ia), (Ib) and (Ic) are the most favorable pathway for VO_3+ C_2H_4 reaction.

For reactions (4a) and (4b), relative Gibbs free energies at 298 K for various intermediates and transition states are obtained by DFT calculations as shown in Figure 12. The optimized geometries of reaction intermediates and transition states are displayed in Figures 13 and 14, respectively. Several reaction channels are found for the generation of products **P3** (H_2O and VO_2C_2) and **P4** (VO_2 and CH_2CO):

R2 → 12 → 12/13 → 13 → or **R2 → 24 → 24/13 → 13 →**

13/14 → 14 → 14/15 → 15 → 15/16 → 16 → 16/17 → 17 → P3 Channel (IIIa)

13/14 → 14 → 14/15 → 15 → 15/18 → 18 → 18/17 → 17 → P3 Channel (IIIb)

13/22 → 22 → 22/21 → 21 → P4 Channel (IVa)

13/14 → 14 → 14/23 → 23 → P4 Channel (IVb)

13/19 → 19 → 19/20 → 20 → 20/21 → 21 → P4 Channel (IVc)

R2 → 24 → 24/21 → 21 → P4 Channel (IVd)

In the first step, C_2H_2 attacks the V atom of VO_3 cluster to form intermediate **12** or attacks an O atom of VO_3 to form intermediate **24**. As the C-V bond forms, one O atom migrates from VO_3 to C_2H_2 to yield **13** via transition state **12/13** or **24/13**. During this process, the C≡C bond of C_2H_2 is weakened to a C=C bond. After several steps, hydrogen atoms transfer from C atoms to the O atom as in channel (IIIa) and (IIIb), **13** transforms to intermediate **17,** in which H_2O attaches to VOC_2O by a binding energy of ca. 1 eV, and finally, H_2O leaves to generate product **P3** (H_2O + VO_2C_2). Other pathways for the reaction VO_3+ C_2H_2 are viable such that intermediate **13** changes structure to intermediate **21** or **23** via H transfer from one C to another C atom, forming CH_2CO. Channels (IVa), and (IVb) yielding product **P4** are possible. In channel (IVc), a five membered ring structure of intermediate **19** (containing two C-O bonds) is formed. One V-O bond breaks to result in an O atom transfer from VO_3 to C_2H_2. The C-O bond cleavage of **20** yields **21**, which leads to final product **P4**. A barrier (0.167 eV) is found for oxygen abstraction channel (IVd), in which oxygen atom directly transfers from VO_3 to C_2H_2. As illustrated in Figure 12, the barrier heights for water formation (reaction 4a) and ketene (CH_2CO) formation (reaction 4b) are lower than that of the reactant **R2**, indicating that reactions (4a) and (4b) can occur at room temperature.

6. Discussion

A. Association reactions of V_mO_n with C_2H_6, C_2H_4 and C_2H_2

Association reactions are found to be the main reaction channels for vanadium oxide clusters and C_2 hydrocarbons. As shown in Figures 3, 5, and 7, with 118 nm ionization, $V_2O_5C_2H_6$ is the only product identified for the V_mO_n + C_2H_6 reaction. $VO_2C_2H_4$, $V_2O_5C_2H_4$, $V_3O_6C_2H_4$ and $V_3O_8C_2H_4$ are the association products identified for the V_mO_n + C_2H_4 reaction, and $VO_2C_2H_2$, $VO_2C_4H_4$, $V_2O_3C_2H_2$, $V_2O_4C_2H_2$, $V_2O_5C_2H_2$ $V_3O_8C_2H_2$, $V_4O_9C_2H_2$, etc. are the products identified for the V_mO_n + C_2H_2 reaction. Unsaturated hydrocarbons C_2H_2 and C_2H_4 are more reactive with neutral

vanadium oxide clusters than is the saturated hydrocarbon C_2H_6. More association products are observed for the $V_mO_n + C_2H_2$ reaction than for the $V_mO_n + C_2H_4$ reaction. Almost all V_mO_n clusters can form association products with C_2H_2, while most association products come from oxygen rich clusters and the most stable cluster of a given V_m family for the $V_mO_n + C_2H_4$ reaction. We conclude that C_2H_2 is more reactive than C_2H_4 for association reactions with V_mO_n.

The observed reactivity tendency of C_2 hydrocarbons in association reactions with neutral V_2O_5 is consistent with the calculated results. As shown in Figure 8, the saturated hydrocarbon C_2H_6 bonds weakly 0.65 eV with V_2O_5, while C_2H_4 and C_2H_2 bond with V_2O_5 by CO and VC chemical bonds at 1.33 and 2.5 eV, respectively. Based on calculations, the association reactions of $V_2O_5 + C_2H_4/C_2H_2$ to generate $V_2O_5C_2H_4$ and $V_2O_5C_2H_2$ (type A, singlet) are barrierless processes at room temperature. These binding energies are consistent with the experimental observation that the depletion rates for V_2O_5 signals in the mass spectrum increase from C_2H_6, C_2H_4, to C_2H_2. As shown in Figure 3, a small depletion of the V_2O_5 signal and a weak new $V_2O_5C_2H_6$ signal are observed when C_2H_6/He gas is added in the reactor cell, implying a slow reaction rate and weak binding between V_2O_5 and C_2H_6. More than half, and nearly all, of the V_2O_5 signal is depleted if C_2H_4/He (Figure 5) and C_2H_2/He (Figure 7) are added in reactor cell, respectively, implying that relatively fast reactions and strong binding occur between V_2O_5 and C_2H_4/C_2H_2. The dissociation rate constant of the association intermediate ($V_2O_5C_2H_x^*$) can be estimated employing the classical Rice-Ramsberger-Kassel-Markus (RRKM) theory: $k_{dissociation} = \nu (1 - E_{bind}/E)^{S-1}$, in which $E_{activation}$ is replaced by E_{bind}, the binding energy of ($V_2O_5C_2H_x$), ν is the effective frequency of the ($V_2O_5C_2H_x^*$) dissociation coordinate, E is the total energy in ($V_2O_5C_2H_x^*$) (i. e., center of mass collision energy + cluster initial vibrational energy temperature + the association energy[74]), and *S* is the number of oscillators in the ($V_2O_5C_2H_x^*$) intermediate. A higher binding energy implies a slower dissociation rate constant and thus a longer lifetime for the meta-stable initial association intermediate ($V_2O_5C_2H_x^*$). The $V_2O_5C_2H_x^*$ would eventually fall apart ($V_2O_5 + C_2H_x$) if no further reactions and/or collisions could remove excess energy in the association intermediate ($V_2O_5C_2H_x^*$). In 118 nm flow tube experiments (mixture C_2H_x/He is added into flow tube), the longer lifetime of $V_2O_5C_2H_x^*$

means that the meta-stable species has more chance to be cooled by collisions and thus a higher depletion rate of V_2O_5 cluster will be observed. Although Figure 8 addresses a specific cluster (V_2O_5) association with C_2 hydrocarbons, it reflects a general observation for all V_mO_n clusters. This conclusion supports and is supported by the calculated results given in Figures 10 and 13 [compare $VO_3C_2H_4$ (**3**) with $VO_3C_2H_2$ (**12**), and $VO_3C_2H_4$ (**5**) with $VO_3C_2H_2$ (**19**)], as well as the experimental observations.

We observe association products $V_3O_9C_2H_2$, $V_4O_{11}C_2H_2$, and $V_5O_{14}C_2H_2$ in V_mO_n + C_2H_2 reactions (Figure 6) by 26.5 eV laser ionization; however, oxygen rich clusters, V_3O_9, V_4O_{11}, and V_5O_{14}, are not observed in the vanadium oxide cluster distribution using either 10.5 eV or 26.5 eV ionization. These clusters can not, of course, be detected by 118 nm light due to their high ionization energies, but the photon energy of 26.5 eV light is enough to ionize any neutral cluster. The only explanation for this observation is that small amounts of V_3O_9, V_4O_{11}, and V_5O_{14} are generated in ablation source, and exist in the molecular beam, but they are dissociated via losing O or O_2 during the ionization process by 26.5 eV photons. Based on theoretical calculations,[72] stable structures of V_3O_9, V_4O_{11}, and V_5O_{14} can be found, but they possess O or O-O species that are much more weakly bound relative to O atoms of the most stable clusters, V_3O_7, V_4O_{10}, V_5O_{12}, and even oxygen rich clusters V_3O_8 and V_5O_{13}. Thus, C_2H_2 molecules can apparently stabilize these neutral oxygen rich clusters to avoid cluster fragmentation during the ionization process by forming CO bonds and changing the nature of the oxygen binding in the $V_mO_nC_2H_2$ cluster. The structures in these clusters are presented in Figure 8 (see types B and C).

B. C=C bond breaking in V_xO_{y+1} + C_2H_4 (x =1,3,5,…) reactions

New products VO_2CH_2, $V_3O_7CH_2$, and $V_5O_{12}CH_2$ are observed in the study of the V_mO_n + C_2H_4 reactions as shown in Figures 4 and 5. They can be produced from the following reactions:

$$V_xO_{y+1} + C_2H_4 \rightarrow V_xO_yCH_2 + CH_2O \quad (5)$$

$$V_xO_y + C_2H_4 \rightarrow V_xO_y\,CH_2 + CH_2 \quad (6)$$

in which x =1, 3, 5… In reaction (5), oxygen rich clusters V_xO_{y+1}, such as VO_3, V_3O_8, or V_5O_{13}, react with C_2H_4 and lose a CH_2O molecule. Based on DFT calculations, reaction (1a), $VO_3 + C_2H_4 \rightarrow VO_2CH_2 + CH_2O$, is thermodynamically favorable by 0.3 eV, and is an overall barrierless reaction at a room temperature. Thus, VO_3 can be responsible for the generation of VO_2CH_2. One can then suggest that reaction (5) can also occur and oxygen rich clusters (V_xO_{y+1}, x = 1, 3, 5…) can cause C=C bond breaking for C_2H_4. Oxygen rich clusters VO_3, V_3O_8, and V_5O_{13} disappear in the TOFMS (see Figure 4(c,d)) if C_2H_4 is added to the flow tube reactor. H_2CO^+ is not detected in these experiments with either 10.5 or 26.5 eV ionizations possibly because the ionization cross section for CH_2O (ionization energy 10.9 eV[75]) is small at 26.5 eV, or because the concentration of the H_2CO product is too low to detect.

In reaction (6), the most stable clusters V_xO_y, such as VO_2, V_2O_5, or V_3O_7, etc., react with C_2H_4, producing products $V_xO_yCH_2$ and CH_2. We calculate ΔH_{298} for the reaction $VO_2 + C_2H_4 \rightarrow VO_2CH_2 + CH_2$ based on following thermodynamic equations,

$$VO_2 + CH_2 \rightarrow VO_2CH_2 \qquad \Delta H_{298} = -3.92 \text{ eV} \qquad (7)$$

$$C_2H_4 \rightarrow CH_2 + CH_2 \qquad \Delta H_{298} = +7.48 \text{ eV}\ [76] \qquad (8)$$

$$VO_2 + C_2H_4 \rightarrow VO_2CH_2 + CH_2 \qquad \Delta H_{298} = +3.5 \text{ eV} \qquad (9)$$

ΔH_{298} for reaction (7) is obtained from our DTF calculation. Reaction (9) is not thermodynamically available at room temperature. Thus, VO_2CH_2 does not arise from reaction (9), and one can then deduce that C=C bond cleavage is not favorable for the most stable vanadium oxide clusters (V_xO_y) as given reaction (6).

$V_xO_yCH_2$ products (see Figure 4) can also arise through fragmentation of association complexes, $VO_2C_2H_4$, $V_3O_7C_2H_4$ and $V_5O_{12}C_2H_4$, caused by 26.5 eV laser ionization. 26.5 eV single photon energy is sufficient to break the C=C bond of $V_xO_yC_2H_4$, to produce $V_xO_yCH_2$ during the ionization process; however, VO_2CH_2 and $V_3O_7CH_2$ products are also observed in 10.5 eV ionization experiments (Figure 5). Single photon energy of 10.5 eV light is not high enough to rupture a C=C bond after ionization. Additionally, using the 26.5 eV laser, the photoionization products of the C_2H_4 molecule are measured as $C_2H_4^+$ (30%), $C_2H_3^+$ (35%), $C_2H_2^+$ (28%), C_2H^+ (3%), CH_2^+ (3%). We do not observe products like $VO_2C_2H_3$ or $V_3O_7C_2H_3$ in the mass spectrum for the V_mO_n +

C_2H_4 reaction, using 26.5 eV light for ionization. Moreover, association complexes $VO_2C_2H_4$, $V_2O_5C_2H_4$, and $V_3O_8C_2H_4$ are observed in the 26.5 eV ionization mass spectrum (see Figure 4). Thereby, $V_xO_yCH_2$ products are most probably generated from reaction (5) rather than from the fragmentation of $VO_2C_2H_4$ and $V_3O_7C_2H_4$.

C=C bond breaking and hydrocarbon selective oxidation occur only on oxygen rich neutral vanadium oxide clusters with composition V_xO_{y+1} (x = 1, 3, 5…). Examples from these studies are found for VO_3, V_3O_8, and V_5O_{13}, reacting with C_2H_4. We also investigate the reactions of niobium and tantalum oxide clusters with C_2H_4; however, C=C bond breaking for C_2H_4 does not occur on Nb_xO_{y+1} or Ta_xO_{y+1} oxygen rich clusters. For oxygen deficient V_xO_{y-1} and stable clusters V_xO_y, only association reaction channels are identified. For vanadium oxide cluster cations reacting with C_2H_4,[33] the identified reaction channels are association and oxygen transfer. The reactions of $V_mO_n^-$ anions with C_2H_4 have also been investigated, but no reaction products are found.[33]

The cleavage of C=C bonds is a very important process for condensed phase catalysis. Formaldehyde is generated in reaction (5) and it is one of the most important fundamental industrial chemicals.[11] The mechanism of C=C bond breaking on VO_3 can be interpreted based on our DFT results shown in Figures 9-11. The first step of the process involves C-O and/or V-C bond formation, as well as C=C bond weakening to form intermediates **3** or **10** (Figure 9). The C=C double bond in CH_2=CH_2 (bond length = 0.1326 nm) is significantly weakened to become a single bond in **2**, **3** or **10** with C-C distances about 0.15 nm (C-C bond length = 0.1527 nm in C_2H_6). The second step in this development is the formation of a second C-O bond leading to the formation of a quite stable five membered intermediate **5** (Figure 10), in which sufficient energy is released to break the C-C bond (**5** → **5/6** → **6**). The formation of intermediate **5** is a key step for C=C bond cleavage. For VO_3, about 2.12 eV energy is released through intermediate **5** formation since the unstable oxidation states of VO_3 is stabilized by the formation of intermediate **5**: the oxidation state of V and O are (+4) and (-2), respectively, in this intermediate. Only 1.3 eV is released, however, as V_2O_5 forms the same five membered ring association product as shown in Figure 8 (type C).

In the process of formaldehyde formation, acetaldehyde (CH_3CHO) formation is also possible. This latter reaction involves a hydrogen atom transfer from one carbon to another as in reaction channels (IIa-e); however, the transfer barrier is high, as shown in Figure 9, so that acetaldehyde formation can only happen at high temperature. The reactions of cationic vanadium oxide clusters ($V_mO_n^+$) with ethylene have been studied by both experiments[25,33,77] and DFT calculations.[33,38] Formaldehyde formation does not occur on $V_mO_n^+$ clusters. In contrast, acetaldehyde formation is found over VO_2^+ [77] and $(V_2O_5)_n^+$, n =1-3,[25,33] and this observation is supported by the DFT calculations.[33,38] Hydrogen transfer barriers in these cationic species are around 0.13 eV – 1.45 eV depending on the reaction intermediates through which the transfer proceeds. In the neutral species studied in this work (Figure 9), hydrogen transfer barriers (0.84 – 2.32 eV) are relatively high. Theoretical explanation of the C=C bond breaking process over $V_mO_n^+$, not taken into account in the previous calculations,[33,38-40] would be interesting to study.

These results for neutral vanadium oxide clusters suggest the question: why does C=C bond breaking only happen on oxygen rich vanadium oxide clusters with an odd number of vanadium atoms, V_xO_{y+1} (x = 1,3,5…)? Based on DFT calculations[72] of the VO_3 structure shown in Figure 15, three oxygen atoms are individually bonded to the V atom with 1.67 Å bond lengths, which value is close to the double bond length of V=O in VO_2 (1.63 Å). Assuming that all the oxygen atoms are in the (-2) oxidation state, the V atom in VO_3 would have an oxidation state greater than its most stable oxidation state (+5); if this is not true, the oxidation state of O atoms would be less negative than (-2). In any case, neutral VO_3 is a very active oxide. In the mass spectrum, detected VO_3 has attached H atoms to stabilize its structure as $VO_3H_{1,2}$. In these $V_mO_nH_x$ clusters, the V atom is in oxidation state (+5/+4) and O atoms are in oxidation state (-2). Additionally, DFT calculation shows that VO_3 associates with C_2H_4 to form a stable intermediate **5** (Figure 8) to release a large amount of energy (2.12 eV), leading to C=C bond breaking. Oxidation of C_2H_4 by VO_3 to produce VO_2CH_2 and H_2CO is an overall barrierless process at room temperature (Figure 9). In the cluster V_3O_8 (shown in Figure 15), two vanadium atoms bonded to three O atoms are in the most stable oxidation state (+5), while the other V atom is bonded to four O atoms with two V-O bond lengths at 1.67 Å

(close to the double bond value) and two V-O bond lengths at 1.82 Å (close to single bond length). A V_3O_8 structure can be generated fromV_2O_5 bonded to VO_3, as a formula $(V_2O_5)(VO_3)$, in which the VO_3 moiety is the active site. Thus, oxygen rich clusters with odd number of V atoms (V_xO_{y+1}, x = 1,3,5,…) can be expressed as $(V_2O_5)_z(VO_3)$. This active VO_3 like structure is not found in either the most stable clusters $(V_2O_5)_z$ or oxygen rich clusters containing an even number of V atoms (V_xO_{y+1}, x=2, 4, 6,…).[72,78] We suggest that the VO_3 moiety can be an active site for neutral vanadium oxide clusters. Evidence for an active moiety in gas phase clusters further validates the idea that active sites of condensed phase oxide catalysts can be effectively modeled with gas phase clusters.

In practical catalysis, the selectivity of hydrocarbon partial oxidation is very important. In this work, we can present a catalytic model for formaldehyde formation through oxidation of C_2H_4 on VO_3. Based on our calculations (B3LP/TZVP), the reaction

$$VO_2CH_2 + O_2 \rightarrow VO_3 + CH_2O \qquad \Delta H_{298} = -2.36 \text{ eV} \qquad (10)$$

is thermodynamically available without a barrier. A catalytic cycle of C_2H_4 oxidation to H_2CO by VO_3 is suggested based on our experiments and theoretical calculations, as presented in Scheme 1.

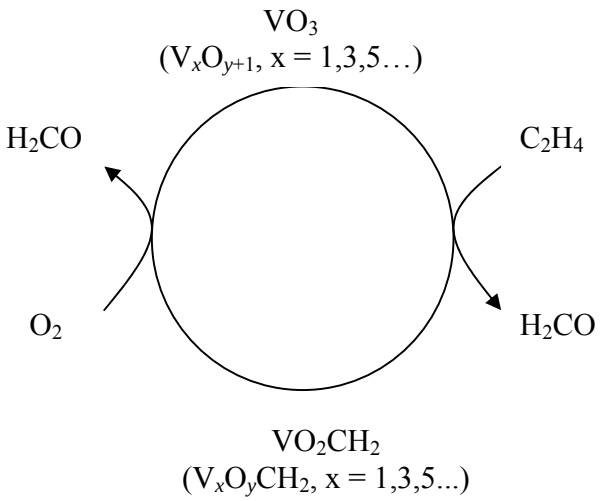

Scheme 1

Since VO_3 can thereby be employed in a catalytic cycle for C_2H_2 oxidation to H_2CO, other larger clusters in this type (V_xO_{y+1}, x = 1,3,5…) can be active in a similar fashion. The understanding of the general characteristics of V_xO_{y+1} (x = odd) would provide a possible opportunity for practical catalyst design for the synthesis of important chemicals (e.g. formaldehyde) through ethylene oxidation,

$$C_2H_4 + O_2 \rightarrow 2CH_2O \qquad \Delta H_{298} = -2.95 \text{ eV}\ ^{76} \qquad (11)$$

Further theoretical investigations on larger clusters are in progress.

C. Dehydration reactions for $V_mO_n + C_2H_2$

Association reactions are the main channels for the reaction of $V_mO_n + C_2H_2$. Additionally, two new products, VO_2C_2 and VOC_4H_2 are observed in Figures 6 and 7. VO_2C_2 can be produced from dehydration reactions (4a) that are thermodynamically and dynamically favorable at room temperature (see Figures 12-14). VOC_4H_2 is suggested to be produced in the following reaction:

$$VO_2 + 2C_2H_2 \rightarrow VO_2C_2H_2 + C_2H_2 \rightarrow VO_2C_4H_4^* \rightarrow VOC_4H_2 + H_2O \qquad (12)$$

Shown in Figures 6 and 7, the strong signals of intermediates $VO_2C_2H_2$ and $VO_2C_4H_4$ are observed as well as an obvious depletion of the VO_2 signal, suggesting that the dehydration reactions (4a) and (12) can occur under the present experimental conditions. Based on binding energy calculations shown in Figures 8, 10, and 13, one can imagine that the vibrational temperature of intermediate $VO_2C_4H_4$ will be high if two acetylene molecules are bonded to VO_2. Some of the intermediates $VO_2C_4H_4$ can be dehydrated to yield products $VOC_4H_2 + H_2O$ (reaction 12), and some can be collisionally cooled to form $VO_2C_2H_2$ and $VO_2C_4H_4$ as observed in mass spectra (Figures 6 and 7).

Other possible reactions for the production of VO_2C_2 and VOC_4H_2 are the elimination of H_2 from $VO_2C_2H_2$ and $VO(C_2H_2)_2$, respectively, as follows:

$$VO_2 + C_2H_2 \rightarrow VO_2C_2 + H_2 \qquad \Delta H_{298} = 0.35 \text{ eV} \qquad (13)$$

$$VO + 2C_2H_2 \rightarrow VOC_2H_2 + C_2H_2 \rightarrow VOC_4H_2 + H_2 \qquad (14)$$

DFT calculations show that ΔH_{298} for reaction (13) is endothermic by 0.35 eV, thus, this reaction will probably not occur under present experimental conditions. No significant

depletion of VO relative to VO_2 is observed when C_2H_2 is added to the reactor, and, no new product signal for reaction intermediate VOC_2H_2 is detected in the mass spectra shown in Figures 6 and 7. Therefore, we suggest that reaction (14) does not occur under in our experiment conditions.

Calculational results show that the reaction mechanism for $VO_3 + C_2H_2$ involves two processes: (1) hydrogen transfer from carbon to oxygen leading to water formation (reaction 4a); and (2) hydrogen transfer from carbon to carbon leading to ketene formation (reaction 4b). The energy barriers for these two processes are lower than the reactant energy as shown in Figure 12. Stable molecules, such as H_2O and CO_2, are always unavoidable byproducts in the selective oxidation of hydrocarbons. The calculated results given in Figures 12-14 indicate that, on a gas phase VO_3 cluster, formation of a "selective oxidation product" (ketene) should be accompanied by a "by product" (water) formation. In a practical catalytic reaction, water formation always involves hydrogen transfer from carbon atoms to oxygen atoms, so the calculated results for reaction (4a) in Figures 12-14 suggest mechanisms for this process. The barrier to hydrogen transfer (**14** – **14/15** – **15**) is around 1 eV if one starts with the unstable species **14** in Figure 13, for which one carbon atom forms only three bonds. The barrier (**16** – **16/17** – **17**) can be as high as ca. 2 eV if one starts from the relatively stable species (**16**). The formed H_2O molecule can adsorb (**17** in Figure 13) on the "surface" with a binding energy around 1 eV.

Note that a stable five membered ring structure (intermediate **19**) also forms in the $VO_3 + C_2H_2$ reaction. This species is similar to intermediate **5** in the $VO_3 + C_2H_4$ reaction. The large amount of energy released in this process can be used to overcome the barriers in the later steps toward products. The C=C bond of intermediate **19** is too strong to break so that V-O bond cleavage leads to O atom transfer followed by dehydration and ketene production reactions. Nonetheless, in the $VO_3 + C_2H_4$ reaction, the C-C single bond of intermediate **5** is relatively easy to break, and this leads to VO_2CH_2 and CH_2O products. Calculations for the $VO_3 + C_2H_2$ system are in agreement with the experimental observation that reaction (4a) takes place to produce VO_2C_2, as observed in the mass spectrum (Figure 6a). Another channel involving ketene formation is also thermodynamically and dynamically favorable at room temperature; however, the direct

oxygen transfer reaction $V_mO_n + C_2H_y \rightarrow V_mO_{n-1} + C_2H_yO$ is hard to identify experimentally in the neutral oxide cluster reactivity study because product V_mO_{n-1} is usually an experimentally generated reactant, and the other product C_2H_yO can be too low in concentration to detect.

7. Conclusions

The reactions of neutral vanadium oxide clusters with ethane, ethylene, and acetylene are investigated employing 26.5 eV soft x-ray laser and 10.5 eV nm laser ionizations coupled with TOFMS for the first time. DFT calculations are applied to explore the mechanism of vanadium oxide cluster reactions with C_2 hydrocarbons. We find experimentally that reactivity for these reactions between neutral vanadium oxide clusters (V_mO_n) increases from C_2H_6, C_2H_4, to C_2H_2. This reactivity is well interpreted based on the behavior of binding energies calculated for the experimental conditions. Association reactions are identified as the major products for the $V_mO_n + C_2H_2$ reactions. Two dehydration products VO_2C_2 and VOC_4H_2 are also identified. DFT calculated results suggest that both reaction channels, dehydration (water formation) and partial oxidation (ketene formation), can occur without an overall reaction barrier for the $VO_3 + C_2H_2$ reaction. For the reaction of $V_mO_n + C_2H_4$, we observe products VO_2CH_2, $V_3O_7CH_2$ and $V_5O_{12}CH_2$, in additional to association products. C=C bond cleavage occurs for C_2H_4 reacting with the oxygen rich neutral clusters VO_3, V_3O_8, and V_5O_{13}. The DFT calculations indicate that the reaction $VO_3 + C_2H_4 \rightarrow VO_2CH_2 + H_2CO$ is thermodynamically favorable and overall barrierless at room temperature. We suggest that the VO_3 moiety can be an active site for neutral vanadium oxide clusters. Another possible reaction channel, acetaldehyde formation, has about a 0.25 eV barrier although this path is thermodynamically more favorable. We conclude that neutral vanadium oxide oxygen rich clusters V_xO_{y+1} (x = odd number) can break the C=C double bond of C_2H_4 to generate H_2CO. Based on experimental data and DFT calculations, a catalytic cycle for selective oxidation of C_2H_4 to produce formaldehyde on VO_3/V_xO_{y+1} (x = odd number) clusters is suggested. Understanding the catalytic characteristics of such clusters will challenge real catalyst design and synthesis. Further theoretical and experimental investigations for larger alkenes reacting with neutral vanadium oxide clusters are in progress.

Acknowledgment
This work is supported by Philip Morris, U.S.A., the U.S. DOE BES program, the NSF ERC for Extreme Ultraviolet Science and Technology under NSF Award No. 0310717, the National Center for Supercomputing Applications under grant CHE070000N, and the Chinese Academy of Sciences (Hundred Talents Fund), and the 973 Programs (Nos. 2006CB932100 and 2006CB806200).

References:

(1) (a) Fierro, J. L. G. Metal Oxides Chemistry and Applications, Taylor & Francis, **2006**; (b) Thomas, Catalytic Processes and Proven Catalysts, Academic Press, New York, **1970**.

(2) Cornils, B.; Herrmann, W. A. Applied Homogeneous Catalysis with Organometallic Compounds, V5l. 1, 2, VCH, Weinheim, **1996**.

(3) Bell, A. T. *Science* **2003**, *299*, 1688.

(4) Schroder, D.; Schwarz, H. *Angew. Chem. Int. Ed. Engl.* **1995**, *34*, 1973.

(5) O'Hair, R. A. J.; Vrkic, A. K.; James, P. F. *J. Am. Chem. Soc.* **2004**, *126*, 12 173.

(6) Waters, T.; O'Hair, R. A. J.; Wedd, A. G. *J. Am. Chem. Soc.* **2003**, *125*, 3384.

(7) Barteau, M. A. *Chem. Rev.* **1996**, *96*, 1413.

(8) Weckhuysen, B. M.; Keller, D. E. *Catal. Today* **2003**, *78*, 25-46.

(9) Martinez-Huerta, M.V.; Gao, X.; Tian, H.; Wachs, I.E.; Fierro, J.L.G.; Banares, M.A. *Catalysis Today*, **2006**, *118*, 179-287.

(10) Dunn, J. P.; Stenger, Jr. H. G.; Wachs, I. E. *Catalysis Today*, **1999**, *51*, 301.

(11)(a) Ertl, G.; Knozinger, H.; Weitkamp, J. Handbook of Heterogeneous Catalysis, Wiley-VCH, Weinheim, **1997**; (b) Banares, M. A.; Alemany, L. J.; Granados, M. L.; Faraldos, M.; Fierro, J. L. G. Catal. Today **1997**, *33*, 73; (c) Herman, R. G.; Sun, Q.; Shi, C.; Klier, K.; Wang, C. B.; Hu, H.; Wachs, I. E.; Bhasin, M. M. Catal. Today **1997**, *37*, 1.

(12) Ogliaro, F.; Harris, N.; Cohen, S.; Filatov, M; de Visser, S. P.; Shaik, S. *J. Am. Chem. Soc*. **2000**, *122*, 8977.

(13) Muetterties, E.L. *Science*, **1977**, *196*, 839.

(14) Bohme, D. K.; Schwarz, H. *Angew. Chem. Int. Ed.* **2005**, *44*, 2336.

(15) Zemski, K.A.; Justes, D.R.; Bell, R.C.; Castleman, A.W., Jr. *J. Phys. Chem. A* **2001**, *105*, 4410.

(16) Schlogl, R.; Hamid, S. B. A. *Angew. Chem. Int. Ed.* **2004**, *43*, 1628.

(17) Bruin, B. de; Budzelaar, P. H. M.; Wal, A. G. *Angew. Chem. Int. Ed.* **2004**, *43*, 4142.

(18) Reuter, K.; Frenkel, D.; Scheffler, M. *Phys. Rev. Lett.* **2004**, *93*, 116105.

(19) Vankoppen, P. A. M.; Brodbeltustig, J.; Bower, M. T.; Dearden, D. V.; Beauchamp, J. L.; Fisher, E. R.; Armentrout, P. B. *J. Am. Chem. Soc.* **1991**, *113*, 2359.

(20) Vankoppen, P. A. M.; Brodbeltustig, J.; Bower, M. T.; Dearden, D. V.; Beauchamp, J. L.; Fisher, E. R.; Armentrout, P. B. *J. Am. Chem. Soc.* **1991**, *112*, 5663.

(21) Vankoppen, P. A. M.; Bower, M. T.; Fisher, E.R.; Armentrout, P. B. *J. Am. Chem. Soc.* **1994**, *116*, 3780.

(22) Zemski, K. A.; Jurtes, D. R.; Castleman, A. W., Jr. *J. Phys. Chem. B* **2002**, *106*, 6136.

(23) Shyue, J.; Guire, M. R. *J. Am. Soc.* **2005**, *127*, 12736.

(24) Feyel, S.; Dobler, J.; Schroder, D.; Sauer, J.; Schwarz, H. *Angew. Chem. Int. Ed.* **2006**, *45*, 4681.

(25) Zemski, K. A.; Justes, D. R.; Castleman, A.W., Jr. *J. Phys. Chem. A* **2001**, *105*, 10237.

(26) Bell, R.C.; Castleman, A.W.Jr.; *J. Phys. Chem. A* **2002**, *106*, 9893.

(27) Zemski, K. A; Bell, R. C.; Castleman, A. W., Jr.; *J. Phys. Chem. A* **2000**, *104*, 5732.

(28) Moore, N. A.; Mitric, R.; Justes, D. R.; Bonacic-Koutecky, V.; Castleman, A.W., Jr. *J. Phys. Chem. B* **2006**, *110*, 3015.

(29) Feyel, S.; Schroder, D.; Schwarz, H. *J. Phys. Chem. A* **2006**, *110*, 2647.

(30) Bell, R. C.; Zemski, K. A.; Castleman, A. W., Jr. *J. Cluster. Sci.* **1999**, *10*, 509.

(31) Bell, R. C.; Zemski, K. A.; Kerns, K. P.; Deng, H. T.; Castleman, A. W., Jr.; *J. Phys. Chem. A* **1998**, *102*, 1733.

(32) Fielcke, A; Rademann, K. *Phys. Chem. Chem. Phys*. **2001**, *4*, 2621.

(33) Justes, D. R.; Mitric, R.; Moore, N. A.; Bonacic-Koutecky, V.; Castleman, A.W., Jr. *J. Am. Chem. Soc*. **2003**, *125*, 6289.

(34) Dobler, J.; Pritzsche, M.; Sauer, J. *J. Am. Chem. Soc.* **2005**, *127*, 10861.

(35) Fielicke A.; Mitric, R.; Meijer, G.; Bonacic-Koutecky, V.; Helden, G. V. *J. Am. Chem. Soc.* **2003**, *125*, 15716.

(36) Cheng, M. J.; Chenoweth, K.; Oxgaard, J.; Duin, A.; Goddard III, W. A. *J. Phys. Chem. C* **2007**, *111*, 5115.

(37) Broclawik, E.; Haber, J.; Piskorz, W. *Chem. Phys. Letts*. **2001**, 333, 332.

(38) Gracia, L.; Sambrano, J. R.; Safont, V. S.; Calatayud, M.; Beltra´n, A.; Andre´s, J. *J. Phys. Chem. A* **2003,** *107,* 3107.

(39) Gracia, L.; Andre´s, J.; Safont, V. S.; Beltra´n, A. *Organometallics* **2004,** *23,* 730.

(40) Gracia, L.; Sambrano, J. R.; Andre´s, J.; Beltra´n, A. *Organometallics* **2006,** *25,* 1643.

(41) Feyel, S.; Schroder, D.; Rozanska, X.; Sauer, J.; Schwarz, H. *Angew. Chem. Int. Ed.* **2006**, 45, 4677.

(42) Gracia, L.; Andres, J; Safont, V.S.; Beltran, A. *Organometallics*, **2004**, *23*, 730.

(43) Gracia, L.; Sambrano, J. R.; Safont, V. S.; Calatayud, M., Beltran, A.; Andres, J; Beltran, A. *J. Phys. Chem. A* **2003**, *107*, 3017.

(44) Futrell, J. H. *Gaseous Ion Chemistry and Mass Spectrometry*, Wiley, New York, **1986**.

(45) Eller, K.; Schwarz, H. *Chem. Rev.* **1991**, *91*, 1121.

(46) Matsuda Y.; Bernstein, E. R. *J. Phys. Chem. A* **2005**, *109*, 3803.

(47) Dong, F.; Heinbuch, S.; Rocca, J. J.; Bernstein, E. R. *J. Chem. Phys.* **2006**, *125*, 164318.

(48) Heinbuch, S.; Dong, F.; Rocca, J. J.; Bernstein, E. R. J. *Chem. Phys*. In press.

(49) Dong, F.; Heinbuch, S.; Rocca, J. J.; Bernstein, E. R. *J. Chem. Phys*. **2006**, *125*, 154317.

(50) Heinbuch, S.; Dong, F.; Rocca, J. J.; Bernstein, E. R. *J. Chem. Phys*. **2006**, *125*, 154316.

(51) Dong, F.; Heinbuch, S.; Rocca, J. J.; Bernstein, E. R. *J. Chem. phys.* **2006**, *124*, 224319.

(52) Matsuda Y.; Bernstein, E. R. *J. Phys. Chem. A* **2005**, *109*, 314.

(53) Matsuda, Y.; Shin, D. N.; Bernstein, E. R. *J. Chem. Phys*. **2004**, *120*, 4142.

(54) Shin, D. N.; Matsuda, Y.; Bernstein, E. R. *J. Chem. Phys*. **2004,** *120*, 4157.

(55) Matsuda, Y.; Shin, D. N.; Bernstein, E. R. *J. Chem. Phys*. **2004**, *120*, 4165.

(56) He, S.-G.; Xie, Y.; Dong, F.; Heinbuch, S.; Jakubikova, E.; Rocca, J. J.; Bernstein, E. R. *J. Chem. Phys.* submitted.

(57) He, S.-G.; Xie, Y.; Guo, Y. Q.; Bernstein, E. R. *J. Chem. Phys.* **2007**, *126*, 194315.

(58) Geusic, M. E.; Morse, M. D.; O'Brien, S. C.; Smalley, R. E; .*Rev. Sci. Instrum.* **1985**, *56*, 2123.

(59) (a) Heinbuch, S.; Grisham, M.; Martz, D.; Rocca, J. J. *Opt. Express* **2005**, ***13***, 4050. (b) Rocca, J. J.; Shlyaptsev, V. N.; Tomasel, F. G.; Cortazar, O. D.; Hartshorn, D.; Chilla, J. L. A. *Phys. Rev. Lett.* **1994,** *73*, 2192. (c) Rocca, J. J. *Rev. Sci. Instrum.* **1999,** *70*, 3799.

(60) Frisch, M. J.; Truchs, G. W; Schlegel, H. B.; et al. *Gaussian 03, Revision C.02, Gaussian*, Inc, Wallingford CT, **2004**.

(61) Becke, A. D. *Phys. Rev. A* **1988**, *98*, 3098.

(62) Becke, A. D. *J. Chem. Phys.***1993**, *98,* 5648.

(63) Lee, C.; Yang, W.; Parr, R. G. *Phys. Rev. B* **1998**, *37*, 785.

(64) Schaefer, A.; Huber, C.; Ahlrichs, R. *J. Chem. Phys.* **1994**, *100*, 5829.

(65) H. B. Schlegel, *J. Comp. Chem.* **3**, 214 (1982).

(66) Peng, C.; Schlegel, H. B. *Israel J. Chem*.**1994**, *33*, 449.

(67) Peng, C.; Ayala, P. Y.; Schlegel, H. B.; Frisch, M. J. *J. Comp. Chem.* **1996**, *17*, 49.

(68) Gonzalez, C.; Schlegel, H. B. *J. Chem. Phys.* **1989**, *90*, 2154.

(69) Gonzalez, C.; Schlegel, H. B. *J. Phys. Chem* **1990**, *94*, 5523.

(70) (a) Boys, F.; Benardi, F. Molecular Physics **1970**, *19*, 553. (b) Rappe, A. K.;

Bernstein, E. R. *J. Phys. Chem. A* **2000**, *104*, 6117.

(71) Calatayud, M.; Andres, J.; Beltran, A. *J. Phys. Chem. A*. **2001**, *105*, 9760.

(72) (a) Jakubikova, E.; Rappé, A. K.; Bernstein, E. R. *J. Phys. Chem.* Submitted. (b) Jakubikova, E. Ph. D Dissertation (May, **2007**).

(73) Schroder, D.; Shaik, S.; Schwarz, H. *Acc. Chem. Res.* **2000**, *33*, 139.

(74). He, S.G.; Xie, Y.; Bernstein, E. R. *J. Chem. Phys.* **2006**, *125*, 164306.

(75) Tao, W.; Klemm, R. B.; Nesbitt, F. L.; Stief, J. L. *J. Phys. Chem.*, **1992**, *96*, 104.

(76) Chase, M.W., Jr. NIST-JANAF Themochemical Tables, Fourth Edition, *J. Phys. Chem. Ref. Data, Monograph 9*, **1998**, 1-1951.

(77) Harvey, J. N.; Diefenbach, M.; Schro der, D.; Schwarz, H. *Int. J. Mass Spectrom.* **1999**, *182/183*, 85.

(78) Vyboishchikov, S. F. Sauer, J. *J. Phys. Chem. A* **2000**, *46*, 10913.

Figure Captions

Figure 1 Mass spectrum of vanadium oxide clusters ionized by a 26.5 eV soft x-ray laser. Clusters are generated under a condition of low oxygen concentration (0.5% O_2/He expansion gas mixture).

Figure 2 Reaction of V_mO_n clusters with C_2H_6 studied by 26.5 eV soft x-ray laser ionization. (a) V_mO_n cluster distribution generated with 0.5% O_2/He expansion gas. (b) Pure C_2H_6 added to the flow tube reactor.

Figure 3 Reaction of V_mO_n clusters with C_2H_6 studied by 10.5 eV ionization. (a) pure He gas in the flow tube reactor (b) 20% C_2H_6/He in the flow tube reactor.

Figure 4 Reactions of V_mO_n clusters with C_2H_4 studied by 26.5 eV soft x-ray laser ionization. (a) V_mO_n cluster distribution generated with a 0.5% O_2/He expansion gas. (b) Pure C_2H_4 added to the flow tube reactor. New products of the reaction $V_mO_n + C_2H_4$ are detected. (c, d, e) Expanded mass regions around oxygen rich clusters VO_3, V_3O_8, and V_5O_{13}.

Figure 5 Reactions of V_mO_n clusters with C_2H_4 studied by 118 nm (10.5 eV) laser ionization. (a) V_mO_n cluster distribution generated with a 0.5% O_2/He expansion gas, and added He gas in the flow tube reactor. (b) Mixed 5%C_2H_4/He in the flow tube reactor. The products detected by 10.5 eV laser are similar to those detected by 26.5 eV soft x-ray laser ionization.

Figure 6 Reaction of V_mO_n clusters with C_2H_2 studied by 26.5 eV soft x-ray laser ionization. The V_mO_n cluster distribution is generated by a 0.5% O_2/He expansion (lower spectra). When pure C_2H_2 gas is added to the flow tube reactor, many new products are detected (upper spectra). Major products of the reaction are $V_xO_yC_2H_2$. (a) Small cluster region; (b) Large cluster region.

Figure 7 Reaction of V_mO_n clusters with C_2H_2 detected by 118 nm (10.5 eV) laser ionization. The bottom spectra show the V_mO_n cluster distribution generated by a 0.5% O_2/He expansion gas, with He gas added to the flow tube reactor; the top spectra show the cluster and product distributions arising from the same expansion conditions but with mixed 5%C_2H_4/He gas added to the flow tube reactor. (a) Small cluster region and (b) Large cluster region.

Figure 8 DFT optimized geometries of association products $V_2O_5C_2H_x$, x = 6 (top), 4 (middle), and 2 (bottom). Three types of geometry configurations (A, B, C) are presented. The valves x_1/x_2 below each geometry are the zero-point vibrational energy corrected binding energies, in which x_1 and x_2 are the values for the association species in singlet and triplet spin states, respectively. For C_2H_6 van der Waals association with V_2O_5, the association species in triplet state corresponds to the V_2O_5 fragment in the triplet state. Triplet V_2O_5 is not populated in the experiment, so the binding energies are not determined for this case. See text for details.

Figure 9 DFT calculated relative Gibbs free energies at 298 K for various intermediates and transition states for overall reactions $VO_3 + C_2H_4 \rightarrow VO_2CH_2 + CH_2O$ and $VO_3 + C_2H_4 \rightarrow VO_2 + CH_3CHO$. A one integer ($n$) label denotes a reaction intermediate (stable state) with zero imaginary vibrational frequencies. A two integer (n_1/n_2) label denotes a transition state with only one imaginary vibrational frequency, in which n_1 and n_2 are the two stable states that can transfer to each other though n_1/n_2. Lines between appropriate stable and transition states are drawn and constitute reaction pathways between reactants and products.

Figure 10 DFT optimized geometries of the reaction intermediates in Figure 9. The values x_1/x_2 (in eV) in parentheses below each geometry are Gibbs free energies at 298 K and enthalpies at 0 K relative to reactants (R = VO_3+C_2H_4). In this figure and Figures 11, 13, and 14, many structures have two isomers with nearly identically energies. In this case, only one isomer is plotted except for structure 11, for which 11A and 11B are given to show examples of the isomers.

Figure 11 DFT optimized geometries of the transition states in Figure 9. See Figure 10 caption for explanations.

Figure 12 DFT calculated relative Gibbs free energies at 298 K for various intermediates and transition states for reaction channels $VO_3 + C_2H_2 \rightarrow VO_2C_2 + H_2O$ and $VO_3 + C_2H_2 \rightarrow VO_2 + CH_2CO$. See Figure 9 caption for explanations.

Figure 13 DFT optimized geometries of the reaction intermediates in Figure 12. The values x_1/x_2 (in eV) in parentheses below each geometry are Gibbs free energies at 298 K and enthalpies at 0 K relative to reactants (R = VO_3+C_2H_2). See Figure 10 caption for explanations.

Figure 14 DFT optimized geometries of transition states in Figure 12. The values x_1/x_2 (in eV) in parentheses below each geometry are Gibbs free energies at 298 K and enthalpies at 0 K relative to reactants (R = VO_3+C_2H_2). See Figure 10 caption for explanations.

Figure 15 Lowest energy structures of VO_3 and V_3O_8 taken from reference 72

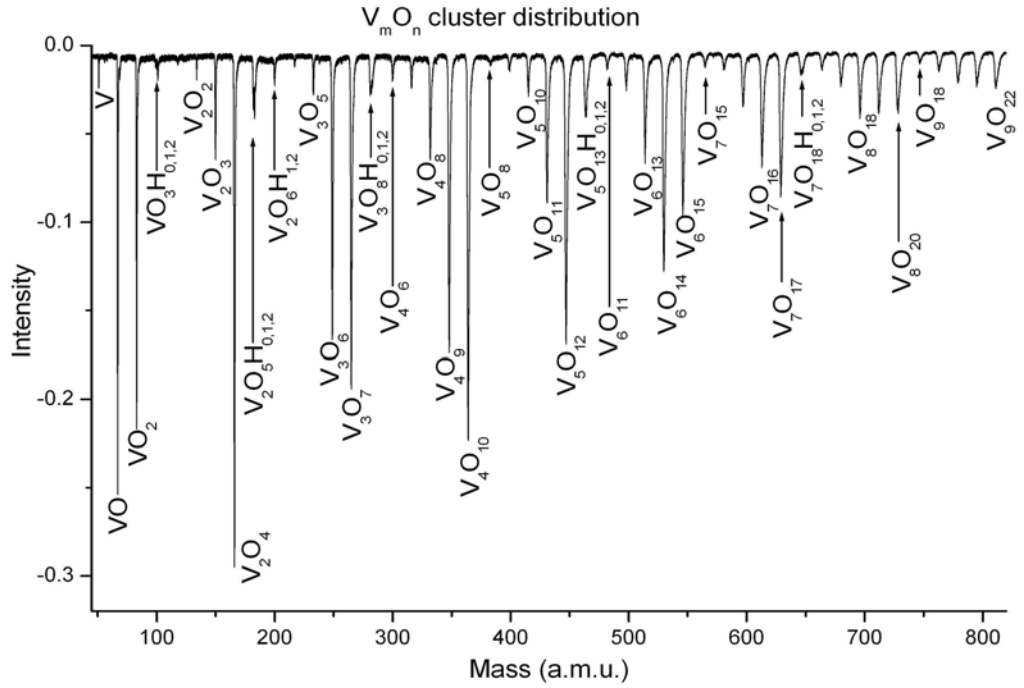

Figure 1

Figure 1 Mass spectrum of vanadium oxide clusters ionized by a 26.5 eV soft x-ray laser. Clusters are generated under a condition of low oxygen concentration (0.5% O_2/He expansion gas mixture).

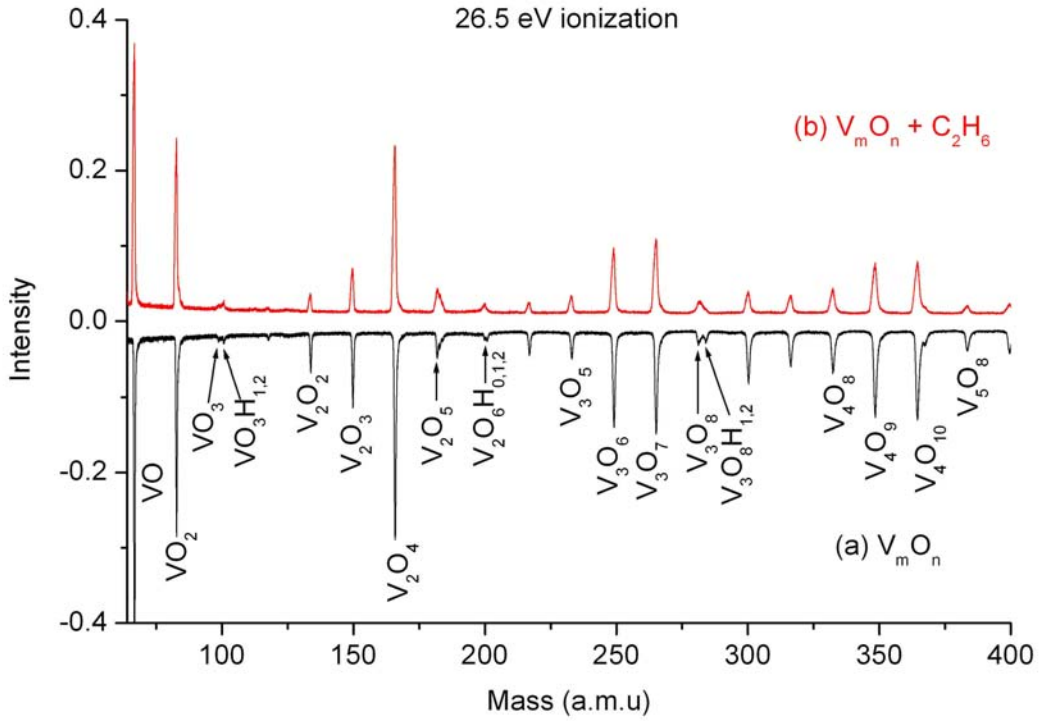

Figure 2

Figure 2 Reaction of V_mO_n clusters with C_2H_6 studied by 26.5 eV soft x-ray laser ionization. (a) V_mO_n cluster distribution generated with 0.5% O_2/He expansion gas. (b) Pure C_2H_6 added to the flow tube reactor.

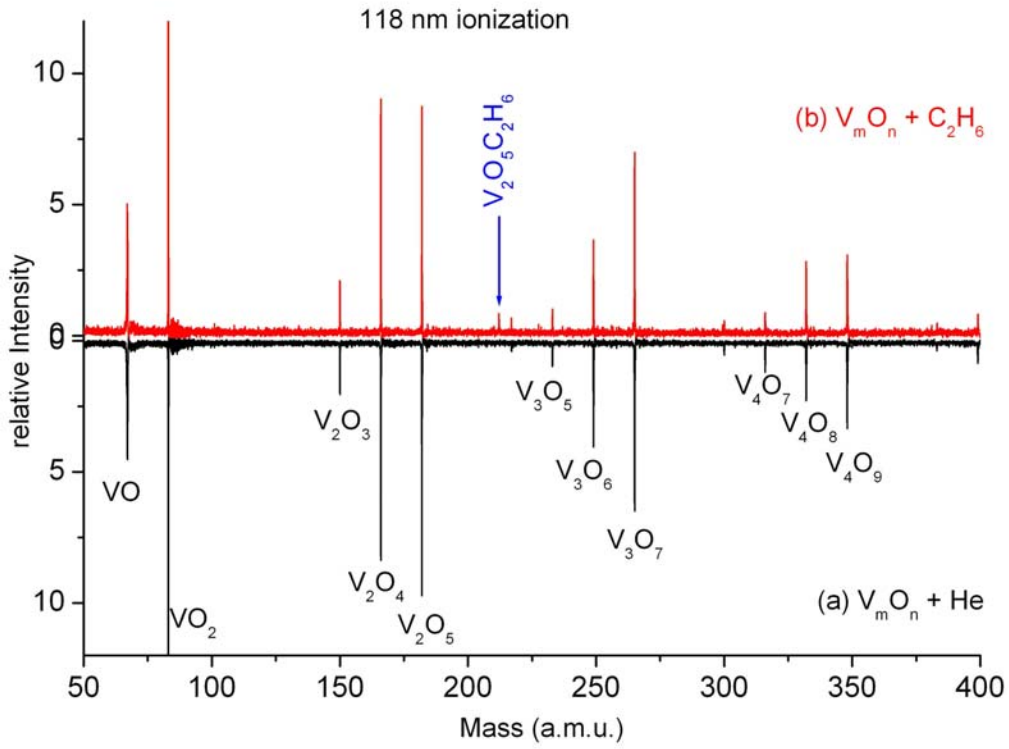

Figure 3

Figure 3 Reaction of V_mO_n clusters with C_2H_6 studied by 10.5 eV ionization. (a) pure He gas in the flow tube reactor (b) 20% C_2H_6/He in the flow tube reactor.

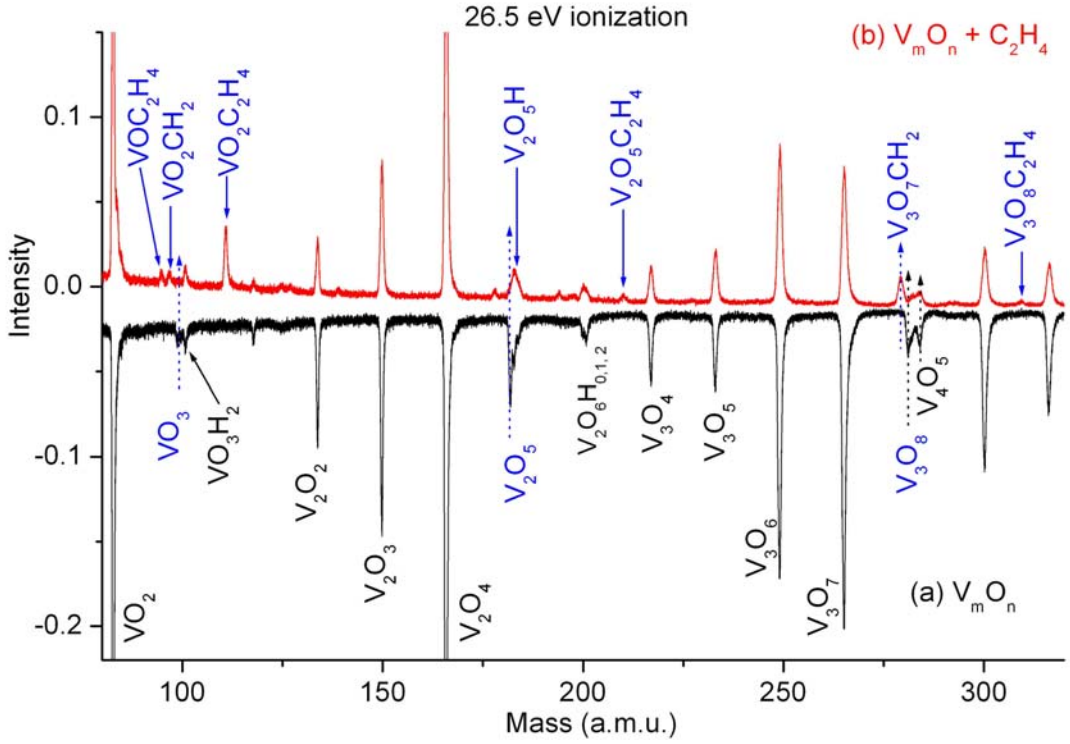
26.5 eV ionization
(b) $V_mO_n + C_2H_4$
(a) V_mO_n
Intensity
Mass (a.m.u.)
0.1
0.0
-0.1
-0.2
100
150
200
250
300
VOC_2H_4
VO_2CH_2
$VO_2C_2H_4$
V_2O_5H
$V_2O_5C_2H_4$
$V_3O_7CH_2$
$V_3O_8C_2H_4$
VO_2
VO_3
VO_3H_2
V_2O_2
V_2O_3
V_2O_4
V_2O_5
$V_2O_6H_{0,1,2}$
V_3O_4
V_3O_5
V_3O_6
V_3O_7
V_3O_8
V_4O_5

Figure 4 (a, b)

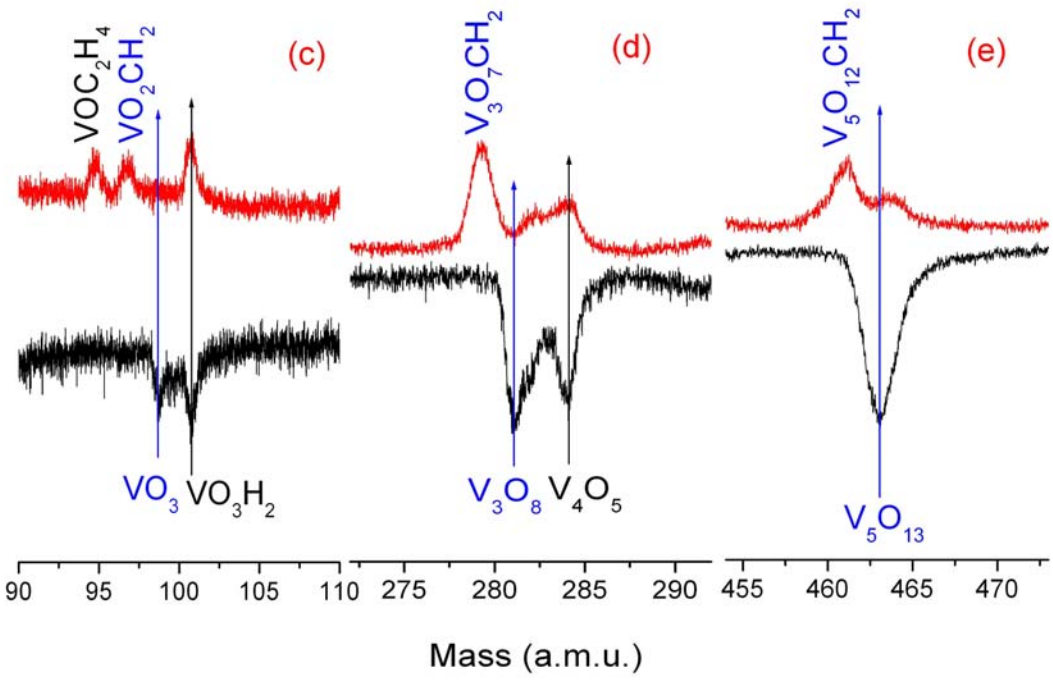

Figure 4 (c, d, e)

Figure 4 Reactions of V_mO_n clusters with C_2H_4 studied by 26.5 eV soft x-ray laser ionization. (a) V_mO_n cluster distribution generated with a 0.5% O_2/He expansion gas. (b) Pure C_2H_4 added to the flow tube reactor. New products of the reaction $V_mO_n + C_2H_4$ are detected. (c, d, e) Expanded mass regions around oxygen rich clusters VO_3, V_3O_8, and V_5O_{13}.

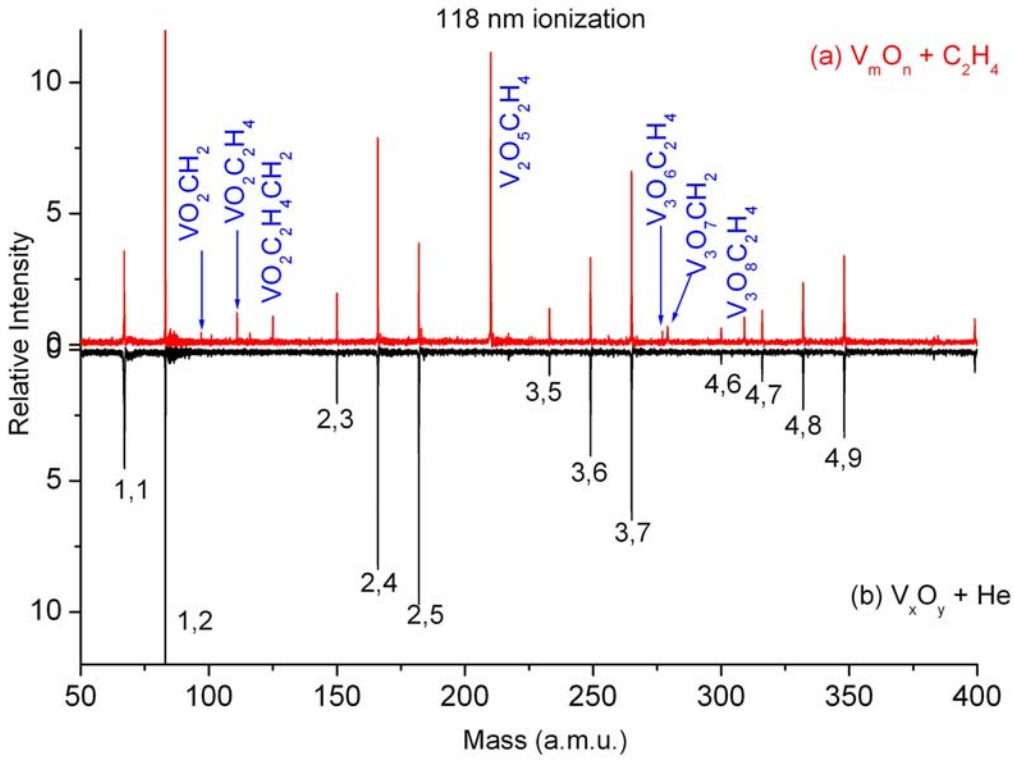

Figure 5

Figure 5 Reactions of V_mO_n clusters with C_2H_4 studied by 118 nm (10.5 eV) laser ionization. (a) V_mO_n cluster distribution generated with a 0.5% O_2/He expansion gas, and added He gas in the flow tube reactor. (b) Mixed 5%C_2H_4/He in the flow tube reactor. The products detected by 10.5 eV laser are similar to those detected by 26.5 eV soft x-ray laser ionization.

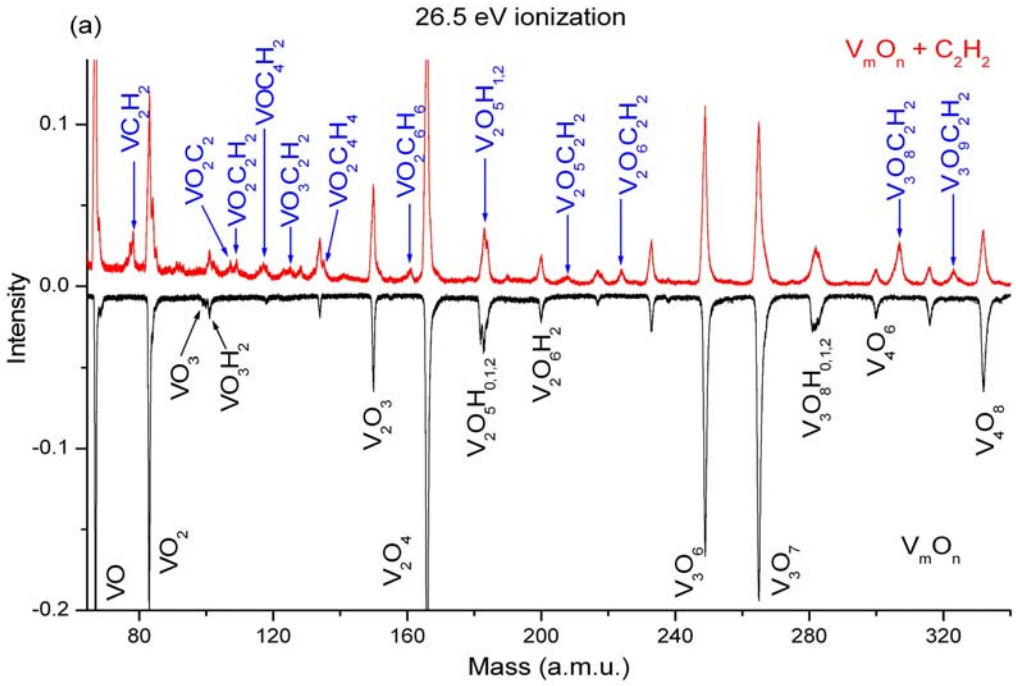
(a)
26.5 eV ionization
$V_mO_n + C_2H_2$
VC_2H_2
VO_2C_2
$VO_2C_2H_2$
VOC_4H_2
$VO_3C_2H_2$
$VO_2C_4H_4$
$VO_2C_6H_6$
$V_2O_5H_{1,2}$
$V_2O_5C_2H_2$
$V_2O_6C_2H_2$
$V_3O_8C_2H_2$
$V_3O_9C_2H_2$
Intensity
0.1
0.0
-0.1
-0.2
VO
VO_2
VO_3
VO_3H_2
V_2O_3
V_2O_4
$V_2O_5H_{0,1,2}$
$V_2O_6H_2$
V_3O_6
V_3O_7
$V_3O_8H_{0,1,2}$
V_4O_6
V_4O_8
V_mO_n
80
120
160
200
240
280
320
Mass (a.m.u.)

Figure 6a

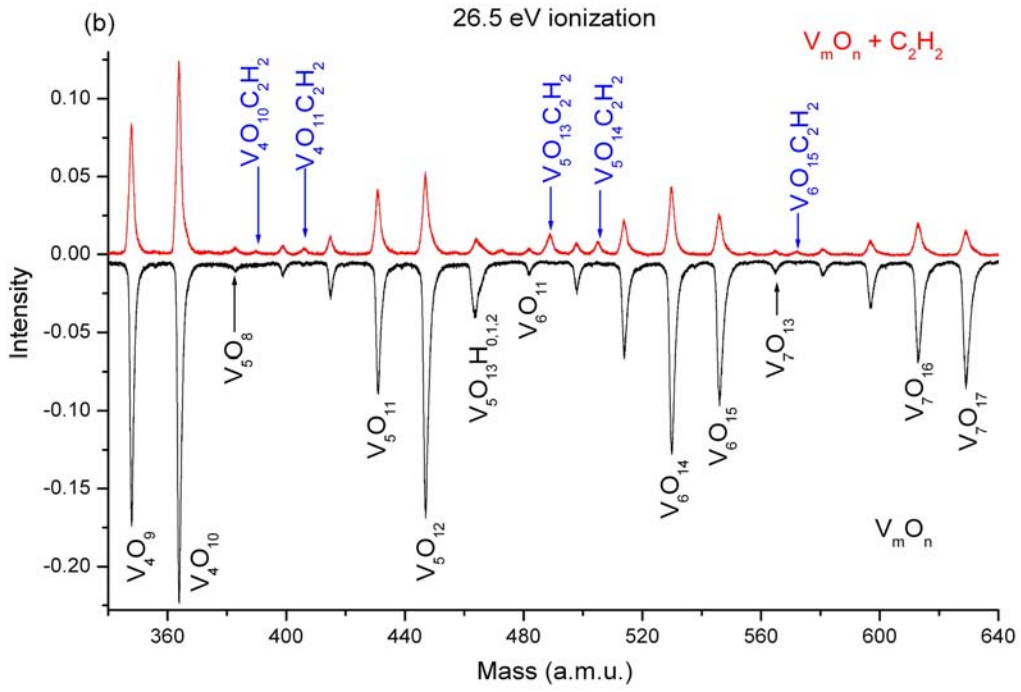

Figure 6b

Figure 6 Reaction of V_mO_n clusters with C_2H_2 studied by 26.5 eV soft x-ray laser ionization. The V_mO_n cluster distribution is generated by a 0.5% O_2/He expansion (lower spectra). When pure C_2H_2 gas is added to the flow tube reactor, many new products are detected (upper spectra). Major products of the reaction are $V_xO_yC_2H_2$. (a) Small cluster region; (b) Large cluster region.

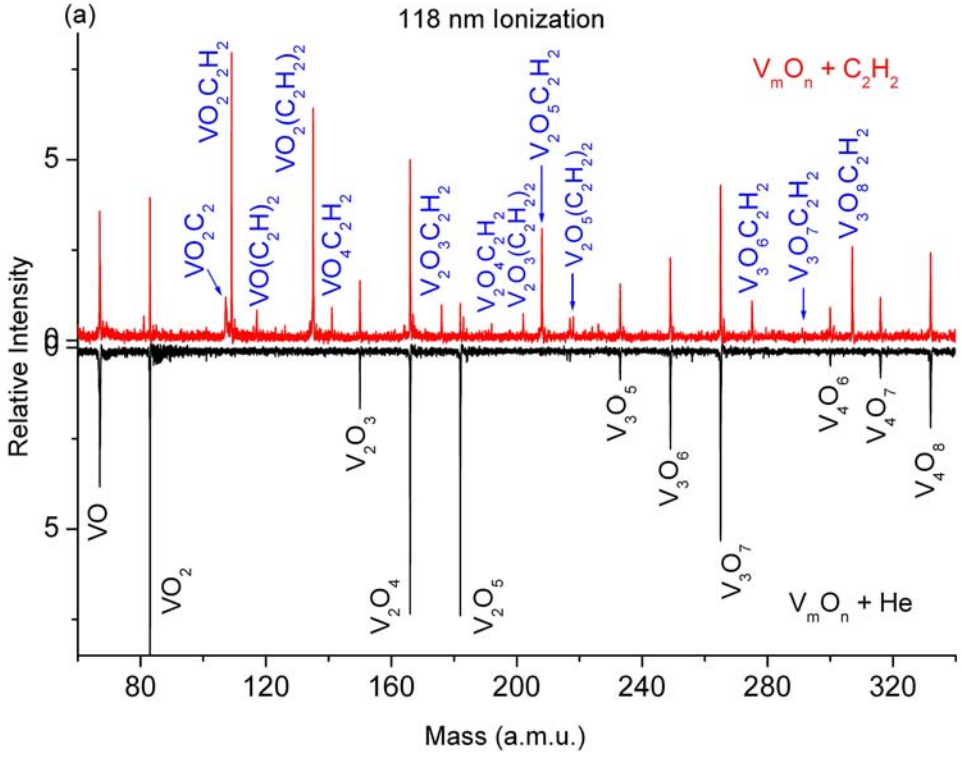
(a)
118 nm Ionization
$V_mO_n + C_2H_2$
$VO_2C_2H_2$
VO_2C_2
$VO_2(C_2H_2)_2$
$VO(C_2H_2)_2$
$VO_4C_2H_2$
$V_2O_3C_2H_2$
$V_2O_4C_2H_2$
$V_2O_3(C_2H_2)_2$
$V_2O_5C_2H_2$
$V_2O_5(C_2H_2)_2$
$V_3O_6C_2H_2$
$V_3O_7C_2H_2$
$V_3O_8C_2H_2$
Relative Intensity
5
0
5
VO
VO_2
V_2O_3
V_2O_4
V_2O_5
V_3O_5
V_3O_6
V_3O_7
V_4O_6
V_4O_7
V_4O_8
V_mO_n + He
80
120
160
200
240
280
320
Mass (a.m.u.)

Figure 7(a)

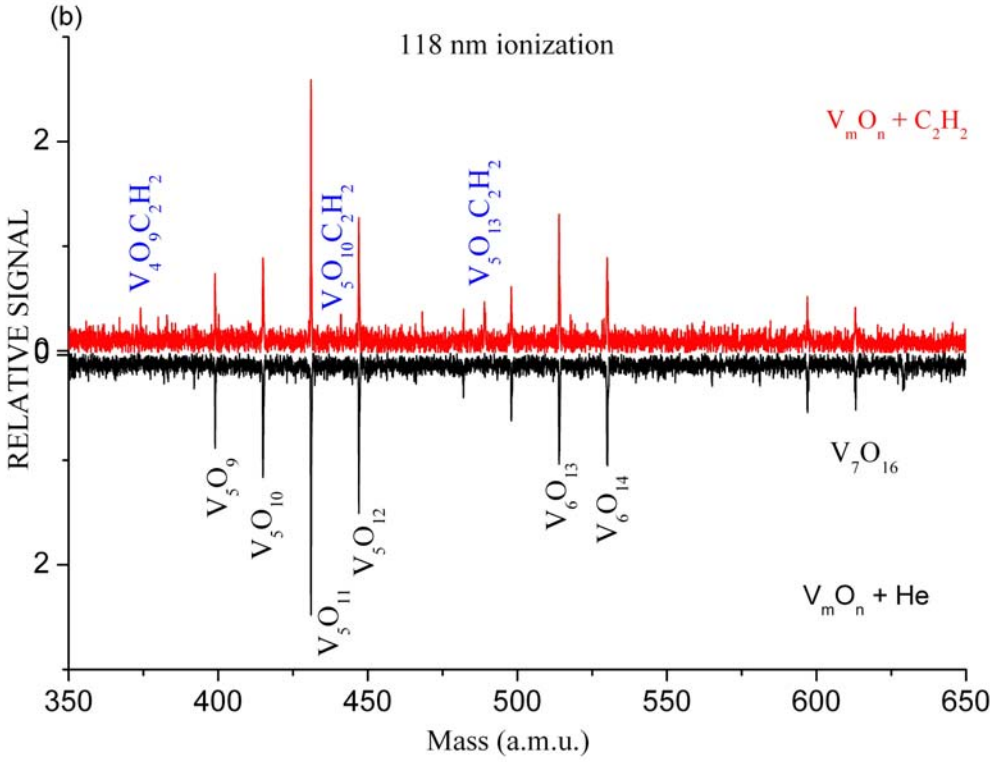

Figure 7b

Figure 7 Reaction of V_mO_n clusters with C_2H_2 detected by 118 nm (10.5 eV) laser ionization. The bottom spectra show the V_mO_n cluster distribution generated by a 0.5% O_2/He expansion gas, with He gas added to the flow tube reactor; the top spectra show the cluster and product distributions arising from the same expansion conditions but with mixed 5%C_2H_4/He gas added to the flow tube reactor. (a) Small cluster region and (b) Large cluster region.

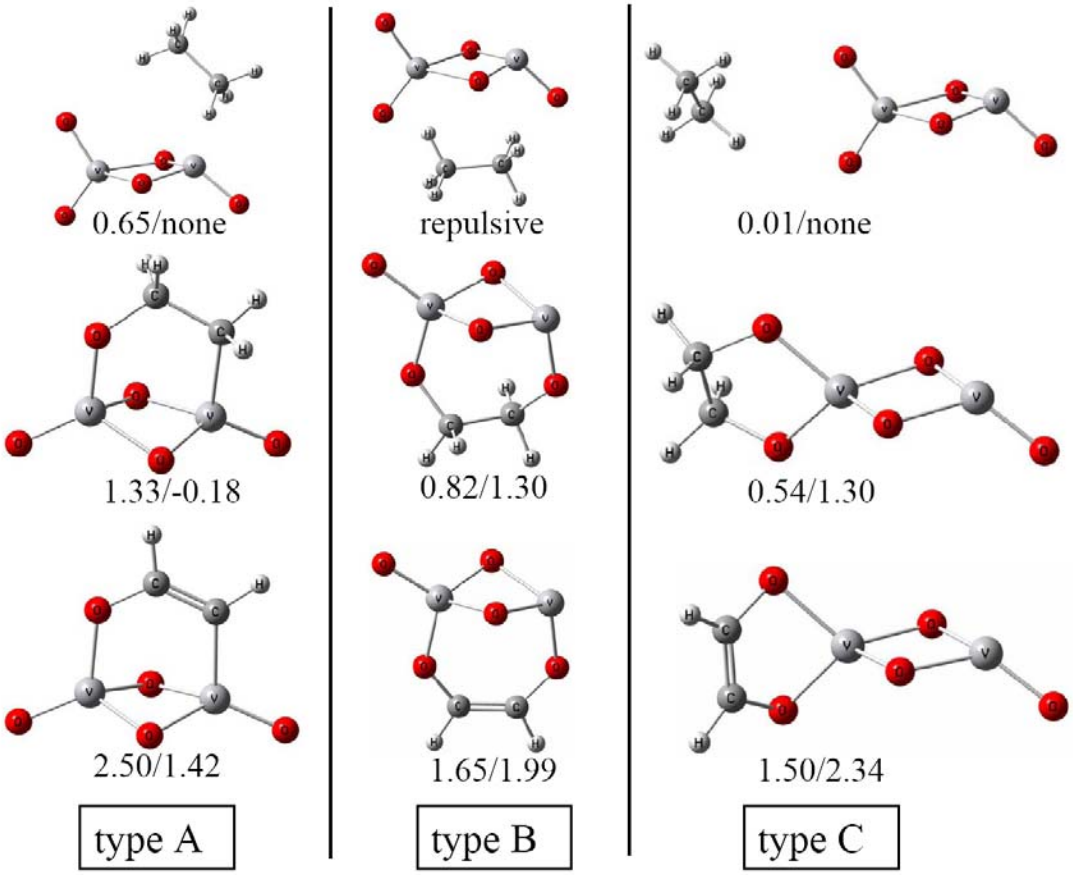

Figure 8 DFT optimized geometries of association products $V_2O_5C_2H_x$, x = 6 (top), 4 (middle), and 2 (bottom). Three types of geometry configurations (A, B, C) are presented. The valves x_1/x_2 below each geometry are the zero-point vibrational energy corrected binding energies, in which x_1 and x_2 are the values for the association species in singlet and triplet spin states, respectively. For C_2H_6 van der Waals association with V_2O_5, the association species in triplet state corresponds to the V_2O_5 fragment in the triplet state. Triplet V_2O_5 is not populated in the experiment, so the binding energies are not determined for this case. See text for details.

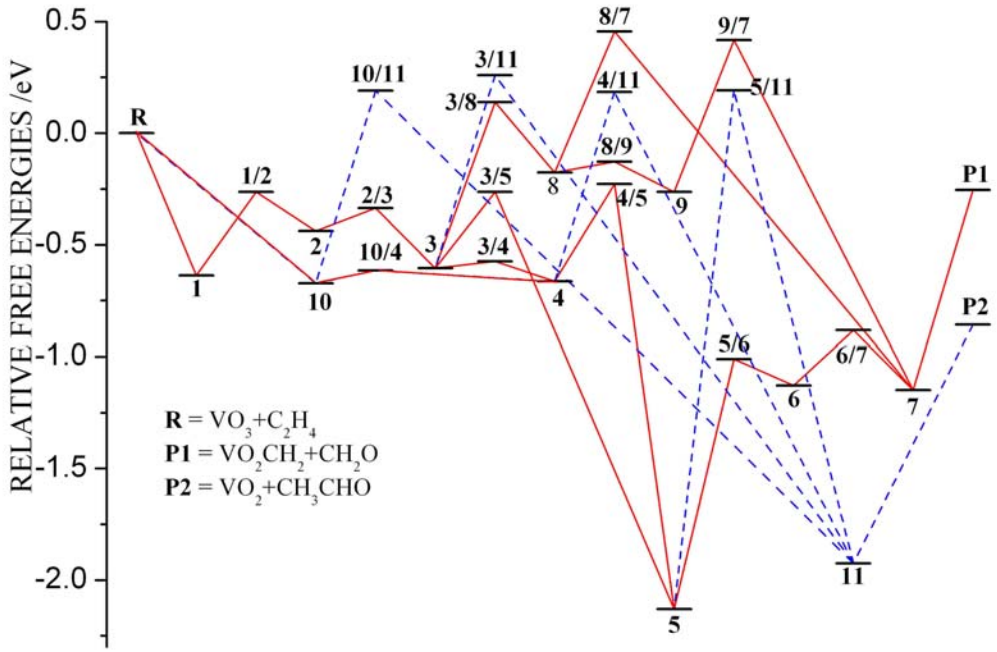

Figure 9 DFT calculated relative Gibbs free energies at 298 K for various intermediates and transition states for overall reactions $VO_3 + C_2H_4 \rightarrow VO_2CH_2 + CH_2O$ and $VO_3 + C_2H_4 \rightarrow VO_2 + CH_3CHO$. A one integer ($n$) label denotes a reaction intermediate (stable state) with zero imaginary vibrational frequencies. A two integer (n_1/n_2) label denotes a transition state with only one imaginary vibrational frequency, in which n_1 and n_2 are the two stable states that can transfer to each other though n_1/n_2. Lines between appropriate stable and transition states are drawn and constitute reaction pathways between reactants and products.

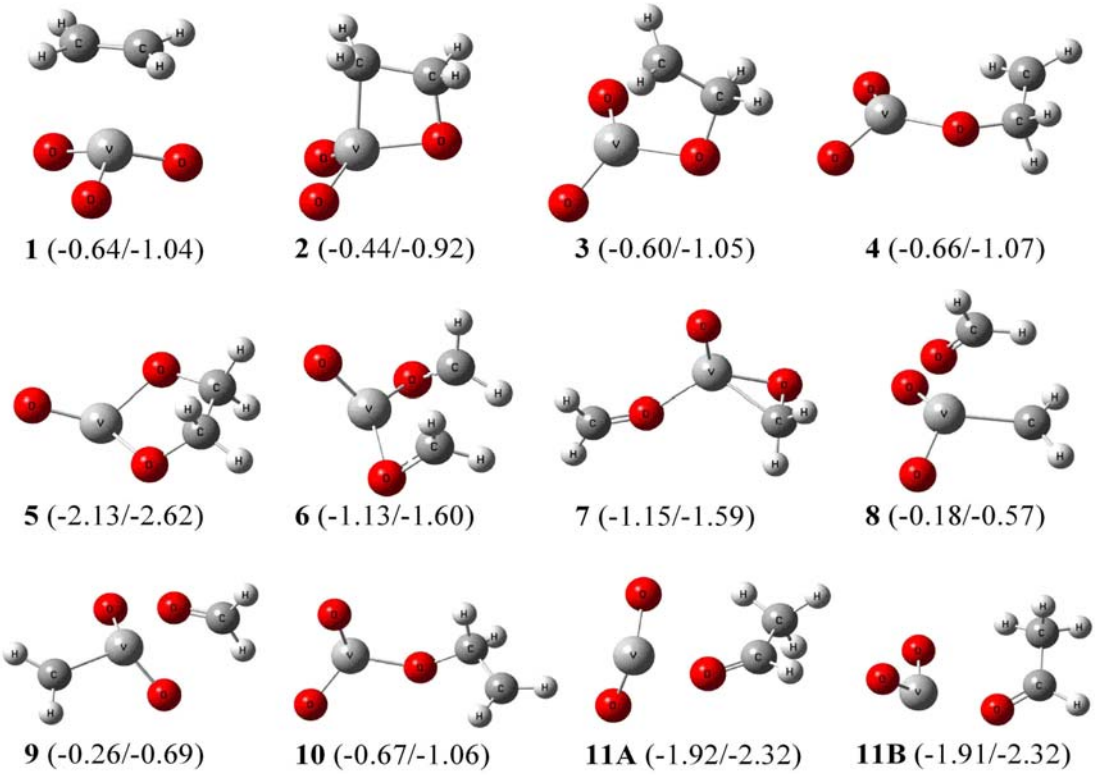

Figure 10 DFT optimized geometries of the reaction intermediates in Figure 9. The values x_1/x_2 (in eV) in parentheses below each geometry are Gibbs free energies at 298 K and enthalpies at 0 K relative to reactants (R = VO_3+C_2H_4). In this figure and Figures 11, 13, and 14, many structures have two isomers with nearly identically energies. In this case, only one isomer is plotted except for structure 11, for which 11A and 11B are given to show examples of the isomers.

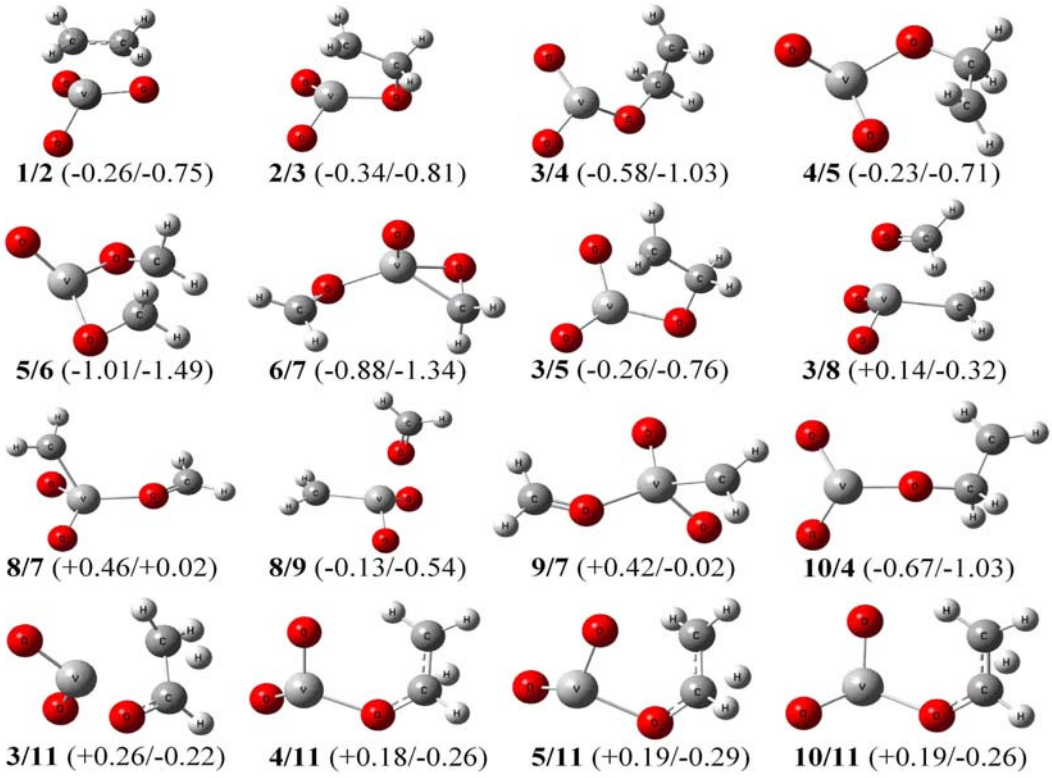

Figure 11 DFT optimized geometries of the transition states in Figure 9. See Figure 10 caption for explanations.

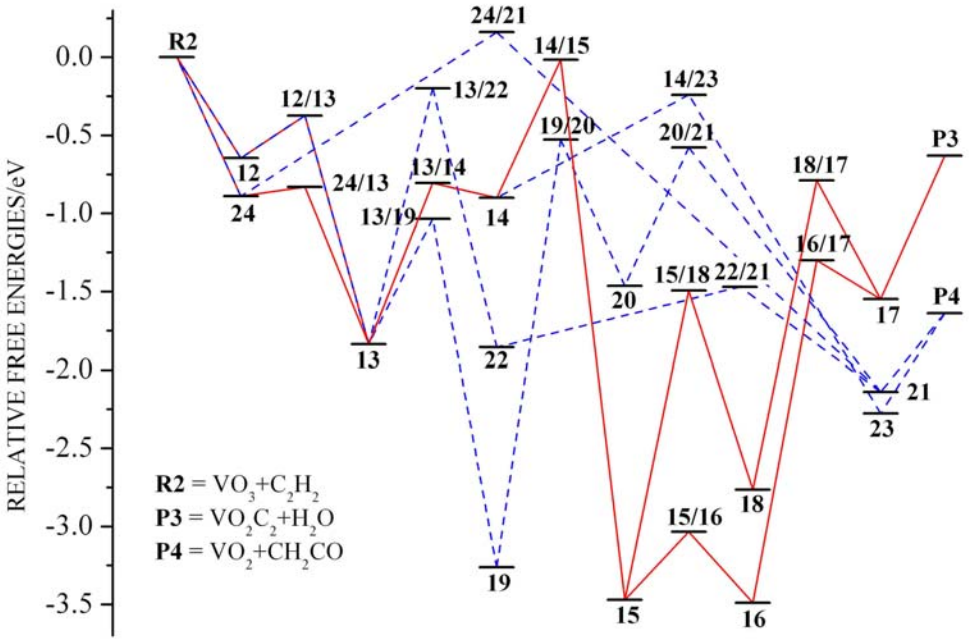

Figure 12 DFT calculated relative Gibbs free energies at 298 K for various intermediates and transition states for reaction channels $VO_3 + C_2H_2 \rightarrow VO_2C_2 + H_2O$ and $VO_3 + C_2H_2 \rightarrow VO_2 + CH_2CO$. See Figure 9 caption for explanations.

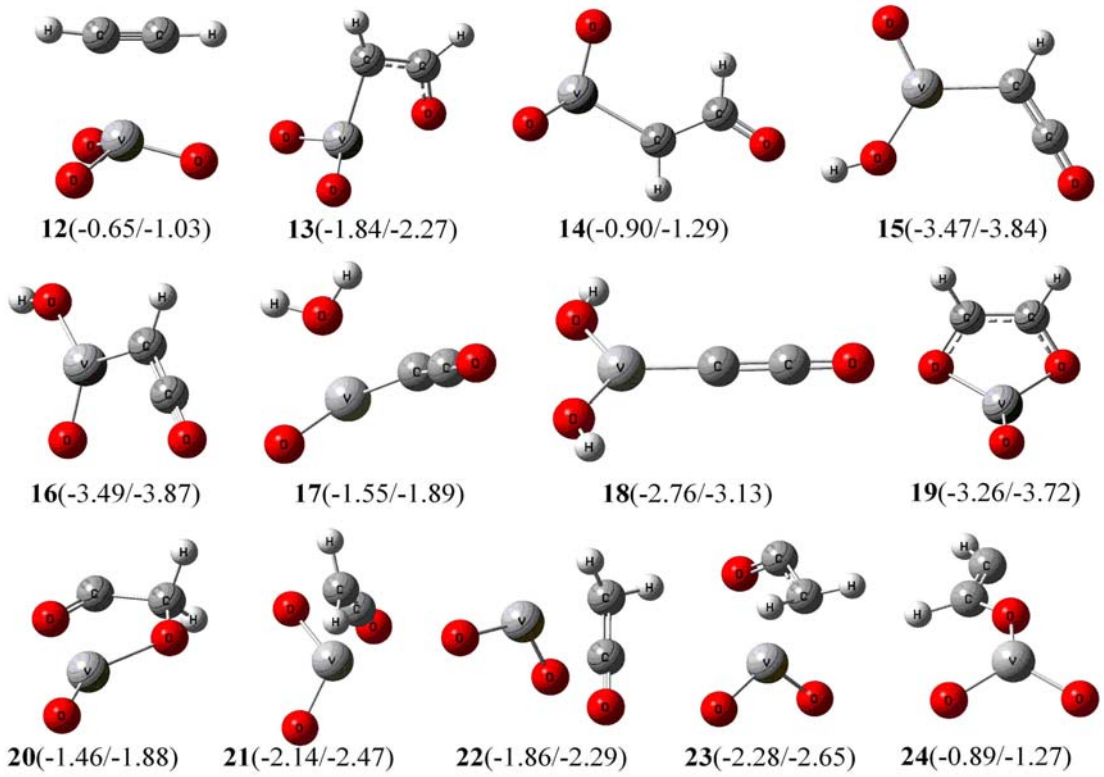

Figure 13 DFT optimized geometries of the reaction intermediates in Figure 12. The values x_1/x_2 (in eV) in parentheses below each geometry are Gibbs free energies at 298 K and enthalpies at 0 K relative to reactants (R = VO_3+C_2H_2). See Figure 10 caption for explanations.

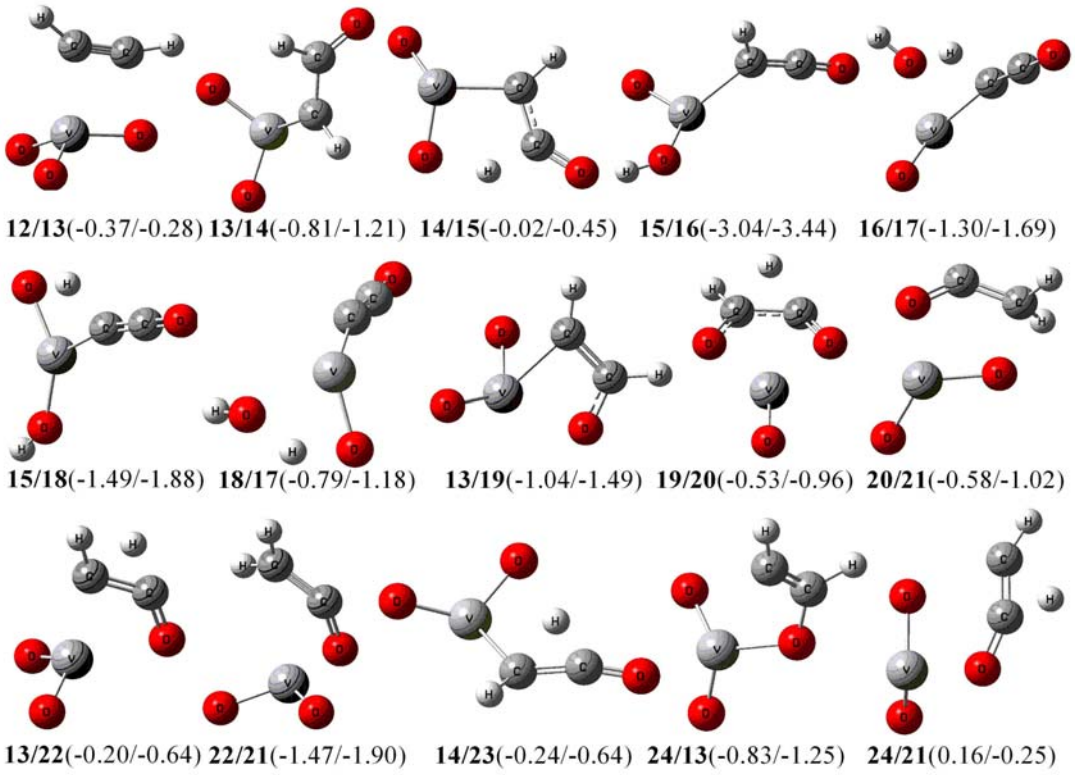

Figure 14 DFT optimized geometries of transition states in Figure 12. The values x_1/x_2 (in eV) in parentheses below each geometry are Gibbs free energies at 298 K and enthalpies at 0 K relative to reactants (R = VO_3+C_2H_2). See Figure 10 caption for explanations.

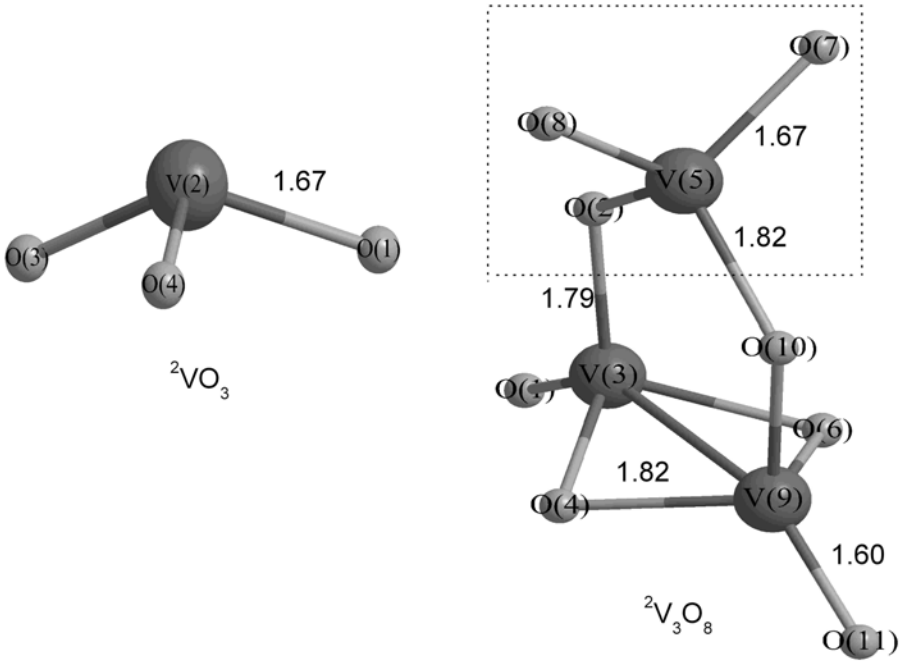

Figure 15 Lowest energy structures of VO_3 and V_3O_8 taken from reference 72

Table of Contents Graphic Instructions